CZECH TECHNICAL UNIVERSITY IN PRAGUE

Faculty of Electrical Engineering
Department of Telecommunication Engineering

Supercontinuum Source in Near- and Mid – infrared Region

Master Thesis

Study Programme: Communications, Multimedia, Electronics
Branch of study: Networks of Electronic Communications

Thesis advisor: Ing. Matěj Komanec, Ph.D.

Suslov Dmytro

Prague 2016

Čestné prohlášení

Prohlašuji, že jsem zadanou diplomovou práci zpracoval sám s přispěním vedoucího práce a konzultanta a používal jsem pouze literaturu v práci uvedenou. Dále prohlašuji, že nemám námitek proti půjčování nebo zveřejňování mé diplomové práce nebo její části se souhlasem katedry.

Datum: 27. 5. 2016

……..……

podpis

Czech Technical University in Prague
Faculty of Electrical Engineering

Department of Telecommunications Engineering

DIPLOMA THESIS ASSIGNMENT

Student: **Bc. Dmytro Suslov**

Study programme: Communications, Multimedia, Electronics
Specialisation: Networks of Electronic Communication

Title of Diploma Thesis: **Supercontinuum Source in Near- and Mind-infrared Region**

Guidelines:

The aim of the thesis is to propose, based on analyses from previous individual project, an optimized configuration for supercontinuum generation with pump wavelength in the vicinity of 1550 nm. A selected microstructured fiber, according to required parameters such as sufficient nonlinearity, transparency and dispersion profile, will be included in the setup. In next step, further experimental part will involve a verification of the proposed setup, generation of the supercontinuum and final comparison with simulation outputs. Supercontinuum generation will be evaluated on at least two different microstructured fibers.

Bibliography/Sources:

[1] Zolla, C.; Renversez, G.; Nicolet, A; Kuhlmey, B.; Guenneau, S.; Felbacq, D.: Foundations of Photonic Crystal Fibres, Imperial College Press, 2005. 376 pages. ISBN: 978-1-86094-507-6.
[2] Dudley, J.M.; Taylor, J.R.: Supercontinuum Generation in Optical Fibers. Cambridge University Press, 04/2010. ISBN: 978-0-521-51480-4.

Diploma Thesis Supervisor: Ing. Matěj Komanec, Ph.D.

Valid until the end of the summer semester of academic year 2016/2017

L.S.

prof. Ing. Boris Šimák, CSc.
Head of Department

prof Ing Pavel Ripka, CSc.
Dean

Prague, December 21, 2015

Summary

This master of science thesis studies linear phenomena in optical fibers, such as chromatic dispersion and nonlinear phenomena, such as Kerr effect, soliton pulse generation, Brillouin and Raman scattering. This thesis studies the properties of their interaction that result in the broadening of optical spectrum – supercontinuum. In this thesis I will study the properties of photonic crystal fibers and their importance to the supercontinuum generation. In simulation part, I will study two chosen fibers. In the end I will experimentally demonstrate supercontinuum generation that will be compared with results from simulations. Conclusion of this thesis contains proposal for further optimization.

Anotace

Tato diplomová práce se zabývá studiem lineárních jevů v optických vláknech, jako je chromatická disperze a nelineárními jevy jako je, Kerrův jev, generace solitonů, Brillouinův a Ramanův rozptyl. Práce se zabývá účinky jejich interakce, které následně vyústí v rozšiřování spektra optického signálu – generaci superkontina. V této práci budu studovat vlastnosti fotonických krystalických vláken a jejích význam pro generaci supercontinua. V simulační části se budu věnovat dvěma zvoleným vláknům. Nakonec bude experimentálně demonstrována generace superkontinua a bude porovnána s výsledky provedených simulací. Závěrem práce je návrh dalšího postupu a optimalizace

Content:

Abbreviations:

GVD	Group Velocity Dispersion
ZDW	Zero Dispersion Wavelength
SPM	Self-Phase Modulation
XPM	Cross-Phase Modulation
SRS	Stimulated Raman Scattering
PCF	Photonic Crystal Fiber
SC	Supercontinuum
SCG	Supercontinuum Generation
FSL	Femtosecond Pulse Laser
VOA	Variable Optical Attenuator
OSA	Optical Spectrum Analyzer
NA	Numerical Aperture
SMF	Single Mode Fiber
EDFA	Erbium-Doped Fiber Amplifier
EDF	Erbium-Doped Fiber
PC	Polarization controller
VLL	Visible Light Laser
SBS	Stimulated Brillouin Scattering
FWM	Four-Wave Mixing
DFWM	Degenerated Four-Wave Mixing
GNLSE	Generalized Nonlinear Schrödinger Equation
NLSE	Nonlinear Schrödinger Equation
GRIN	Graded-Index

1. Introduction

With the development of short pulse lasers, it was possible to introduce high power density optical field to the fiber. That led to high nonlinearity and formation of the supercontinuum [5, 6].

Supercontinuum (SC) itself is an interaction between many nonlinear effects such as the Kerr effect, Raman scattering or solitons. It also utilizes dispersion, which is a linear effect as it does not depend on the input power.

The result of such interaction is a transformation of narrow spectrum signal into a signal with broadband spectrum However, the nature of the interaction of these effects as well as the resulted spectrum depends on the properties of the fiber and the input pulse, such as nonlinearity, input pulse power, input pulse duration and especially group velocity dispersion curve [1, 2, 5, 6, 7].

With the subsequent development of photonic crystal fibers (PCFs), it became possible to precisely tailor these characteristics of PCF to enhance the supercontinuum generation (SCG). Due to the small core area size of PCFs and the pattern of air-filled holes, it is now possible to precisely tailor dispersion profile and simultaneously achieve high nonlinearity [5, 6, 8, 10].

Due to extremely broad spectrum and the pulsed nature of the supercontinuum, it has many applications such as white-light sources in characterization setups, spectroscopy, cellular biology or communications [1, 5, 7].

In this thesis I will first focus on the theoretical description of phenomena connected with SCG and the properties of PCFs. This fundamental knowledge will then be used to describe the interaction of these phenomena in PCF. Based on this theoretical background, I will then summarize the conditions required for SCG from the previous chapters in chapter 4.

In chapter 5 I will choose two available PCFs and design their model using Comsol and Matlab software. I will then use these simulations as estimation of possibility of SCG. Last part of this thesis will then focus on verification of these simulations through the experimental setup.

2. Theoretical background

In this chapter I will study principles of phenomena that influence the supercontinuum generation. The conditions of supercontinuum generation will be discussed in further chapters.

2.1 Dispersion

Dispersion can lead to substantial pulse broadening, especially for ultra-short pulses (below 1 ps). In multimode fibers it is caused by differences in paths of propagating modes or in other words, the differences of their group velocities. In single mode fibers (SMF) with only one propagating mode such phenomenon does not occur. The pulse broadening is still present however, as group velocity of propagating mode is frequency dependent [2].

Dispersion plays a fundamental role in supercontinuum generation. It is a linear effect that influences the character of nonlinear interactions inside a fiber. [1] For the purpose of this paper I will only consider the chromatic dispersion as I will study PCFs. For different fibers such as birefringent fiber or multimode fibers other dispersion properties must be considered [1].

This frequency dependency of fundamental mode in SMF causes different parts (wavelengths) of the pulse launched into fiber to travel at different velocities and is commonly referred to as chromatic dispersion or group velocity dispersion (GVD) [11, 12]. This situation is illustrated in Fig. 2.1.1. [11].

Fig. 2.1.1: Effect of Chromatic dispersion on the wavelength components of the launched pulse [11].

Chromatic dispersion is composed of two components, material dispersion and waveguide dispersion. Material dispersion is based on dependency of refractive index, which is wavelength dependent. Therefore, the pulse launched into fiber that is composed of several wavelengths (characterized by $\Delta\omega$), has each of these wavelengths propagating at different indexes of refractivity. This causes the broadening of the pulse in time domain [2, 3]:

$$\Delta T = L\beta_2\Delta\omega \tag{2.1.1}$$

Where L is fiber length of the fiber, $\Delta\omega$ is frequency difference between spectral components of the optical pulse and β_2 is group velocity dispersion parameter given by [2,3]:

$$\beta_2 = \frac{\delta^2\beta}{\delta\omega^2} \tag{2.1.2}$$

β_2 is therefore a parameter, that determines the amount of the pulse broadening that occurs during a propagation in a fiber [3]. It is customary and more convenient to use the wavelength instead of frequency scale. Therefore, $\Delta\omega$ is often replaced with $\Delta\lambda$ and the resulted pulse broadening is then given by [2, 3]:

$$\Delta T = DL\Delta\lambda \tag{2.1.3}$$

Where *L* is length of fiber, *Δλ* is wavelength difference between spectral components of the optical pulse and *D* is dispersion parameter.

For the final dispersion *D* we can then derive the equation with units of $ps{\cdot}nm^{-1}{\cdot}km^{-1}$ [1, 2, 3]:

$$D = -\frac{2\pi c}{\lambda^2}\beta_2 = -\frac{\lambda}{c}\frac{\delta^2 Re\{n_{eff}\}}{\delta\lambda^2} \tag{2.1.4}$$

We can also define the slope of the dispersion curve as [2, 3]:

$$S = \left(\frac{2\pi c}{\lambda^2}\right)\beta_3 + \left(\frac{4\pi c}{\lambda^3}\right)\beta_2 \tag{2.1.5}$$

Where β_3 is third order dispersion and n_{eff} is effective refractive index. Both equations 1.1.2 and 1.1.4 are complementary definitions of GVD [1]. GVD can achieve several values, if GVD is greater than zero we consider this to be normal dispersion regime whereas if GVD is lesser than zero we consider this to be anomalous dispersion regime [1]. If GVD is equal to zero we refer to it as zero dispersion wavelength (ZDW). The wavelength where ZDW occurs varies based on the fiber structure and fibers can even have several ZDW [1]. For SMF typical value of ZDW is at 1310 nm and the typical dispersion curve can be seen in Fig. 2.1.2. [2].

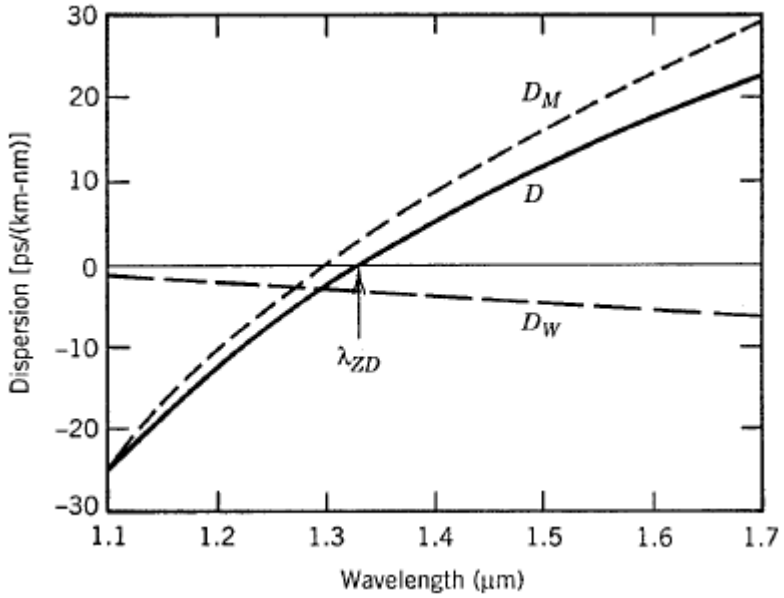

Fig. 2.1.2: Chromatic dispersion of SMF and its components, waveguide dispersion D_W and material dispersion D_M [2].

2.2 Kerr Effect

In practice the refractive index is not only frequency dependent, but also depends on optical power (or intensity of light) [3]. Therefore, optical fiber exhibits nonlinearity when increasing optical power (optical intensity). For refractive index we can derive the equation [2]:

$$n = n_1 + n_2 I \tag{2.2.1}$$

where n_1 is frequency dependent component and n_2 is nonlinear component of the refractive index that depends on light intensity I. As a result, the signal that propagates in a medium (fiber) will change the refractive index of the given medium based upon its own intensity. We can describe this nonlinearity by fiber nonlinearity coefficient γ as [1]:

$$\gamma = \frac{2\pi n_2}{\lambda A_{eff}} \tag{2.2.2}$$

where A_{eff} is effective fiber area. For conventional silica based SMFs γ is in order of 1 – 5 $W^{-1}km^{-1}$. Nonlinear part of refractive index n_2 is much smaller than linear (n_2 in order of 10^{-20} [2]) and therefore at smaller intensities can be neglected [2]. It is important to note, that PCFs have nonlinearity index γ in order of 60 [3, 16], but can achieve even 550 $W^{-1}km^{-1}$ for 1 μm solid core PCFs at 1550 nm [15].

2.3 Effective Area

The optical power intensity leaving the fiber can be simply viewed as the optical intensity leaving the core area of the fiber. However, the problem with such approach is that the distribution of optical intensity is non-uniform and the intensity near the center of the core is higher than at the core-cladding interface and even overlaps into cladding [14]. The example of both Gaussian and rectangular optical field distribution can be seen in Fig. 2.3.1. [13]:

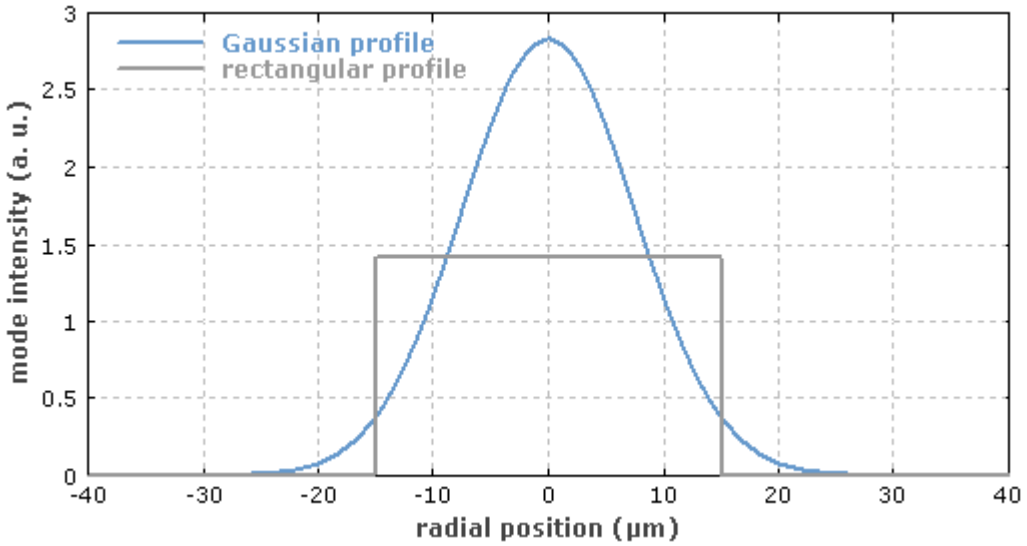

Fig. 2.3.1: Gaussian and rectangular optical intensity distribution for the same effective area [13].

Therefore, the integration is done over the entire fiber area and the effective area is defined as [13, 14]:

$$A_{eff} = \frac{2\pi\left(\int_0^\infty |E_a(r)|^2 r dr\right)^2}{\int_0^\infty |E_a(r)|^4 r dr} = \frac{2\pi\left(\int_0^\infty I(r) r dr\right)^2}{\int_0^\infty I^2(r) r dr} \tag{2.3.1}$$

where $E_a(r)$ is the electric field amplitude and $I(r)$ is the optical field intensity at radius r from the center of the fiber.

2.4 Chirped Gaussian pulse

If we consider a Gaussian pulse propagating in the optical fiber, we can describe it by [2]:

$$A\,(0,t) = A_0 \exp\left[-\frac{1+iC}{2}\left(\frac{t}{T_0}\right)^2\right] \tag{2.4.1}$$

In this equation the A_0 is the peak amplitude, T_0 represents the half-width of the pulse at the 1/*e* and the C is the parameter that is responsible for the frequency chirp of the pulse. That frequency change is then related to the phase by relation [2]:

$$\delta\omega(t) = -\frac{\delta\Phi}{\delta t} = \frac{C}{T_0^2}t \tag{2.4.2}$$

where Φ is the phase of the pulse. If the pulses carrier frequency changes with time as described in equation 2.3.2, we call such pulse to be chirped. Generally, the result of such chirp is broader spectrum of the pulse. However, this is also dependent on the dispersion and in case of $\beta_2 C << 0$ we can observe chirped pulse compression that counteracts the initial pulse chirp and can even negate it completely after certain distance of propagation [2].

If the $\beta_2 C >> 0$ we can observe spectral broadening of the chirped pulse [2]. Broadening of the chirped pulse in relation to propagation distance *z* is then described in relation [2]:

$$\frac{T_1}{T_0} = \left[\left(1 + \frac{C\beta_2 z}{T_0^2}\right)^2 + \left(\frac{\beta_2 z}{T_0^2}\right)^2\right]^{1/2} \tag{2.4.3}$$

Where T_1 is half-width of the pulse at 1/*e* for the broadened pulse, T_0 represents the half width of the original pulse at 1/*e*, β_2 is group velocity dispersion and *C* is the pulse chirp parameter.

In reality we cannot always assume a Gaussian shaped pulse and non-Gaussian shaped pulses can exhibit a large spectral broadening of the pulse. As such we need to modify the equation 2.3.1 to include the shape of the pulse [2]:

$$A\,(0,t) = A_0 \exp\left[-\frac{1+iC}{2}\left(\frac{t}{T_0}\right)^{2m}\right] \tag{2.4.4}$$

The parameter *m* then controls the shape of the pulse. For Gaussian shaped pulse the parameter *m* corresponds to 1. With increasing *m* the pulse becomes almost rectangular and is often called super-Gaussian pulse. Such pulses then tend to broaden more rapidly than Gaussian shaped pulses [2].

2.5 Self-Phase and Cross-Phase modulation

Self-Phase Modulation (SPM) is a nonlinear effect that is directly resulting from Kerr effect. The result is that propagation constant becomes power dependent and can be derived from equation 2.2.1 as [2]:

$$\beta' = \beta + k_0 n_2 \frac{P}{A_{eff}} = \beta + \gamma P \tag{2.5.1}$$

where *γ* is fiber nonlinearity coefficient, P is optical power propagating in the fiber and β is power independent propagation constant. The nonlinear refractive index causes the non-linear phase shift. That phase shift is described by [2,3]:

$$\Phi_{NL} = \int_0^L (\beta' - \beta) dz = \gamma P L \tag{2.5.2}$$

where *P* is optical power propagating in the fiber and L is the length of fiber.

Due to the time variation of optical power presented in equation 2.4.2 the phase of the signal propagating in a fiber also varies with time. This nonlinear phase modulation is induced by the propagating signal on itself and therefore it is called self-phase modulation (SPM) [2] and can be viewed in Fig. 2.5.1. [17].

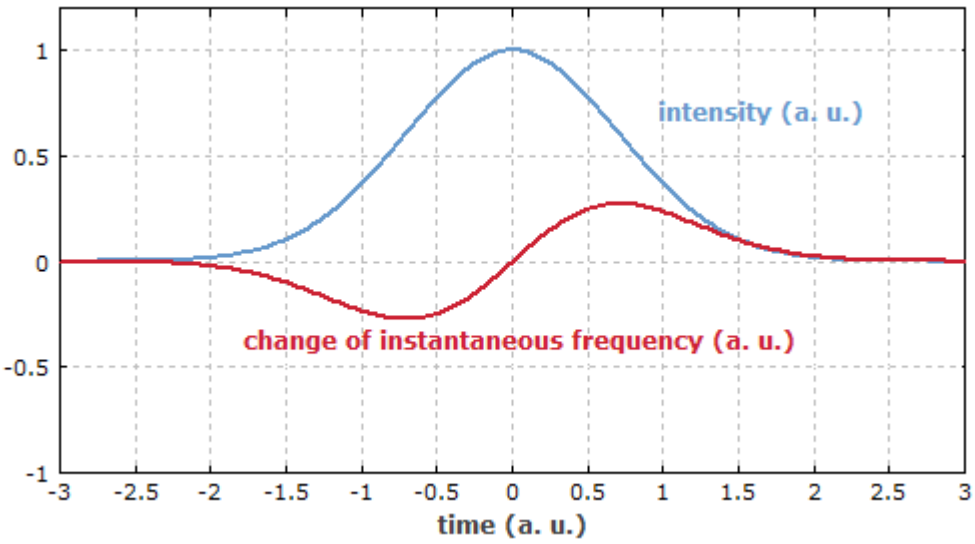

Fig. 2.5.1: SPM induced instantaneous frequency chirp [17].

Similar phenomenon can occur when two (or more) signals propagate in the same fiber. The nonlinear phase shift of a given signal propagating in the fiber would then be dependent on the sum of the power of all the other signals in the fiber. This relation can be described for nonlinear phase shift of the *n*-th channel by equation [2]:

$$\Phi_n^{NL} = \gamma L \, (P_n + 2 \sum_{m \neq \mathrm{n}} Pn) \tag{2.5.3}$$

Where *γ* is fiber nonlinearity coefficient P_n is the optical power of the given signal for the phase shift and the sum is then over the number of the signals. Since different signals induce a nonlinear phase shift, we call this phenomenon cross-phase modulation (XPM) [2, 3].

The important result of both SPM and XPM is the pulse chirping and the resulting spectral broadening of the propagating pulse. However, the effect of the dispersion has to be considered, which results into two distinct modes of operation. In SPM and normal dispersion, the spectral and temporal broadening occurs.

In the second, the interaction of SPM and anomalous dispersion lead to the balance of pulse compression caused by SPM chirp and spectral broadening caused by anomalous dispersion, which results in creation of solitons [1].

The effects of XPM are more complex as they require low group velocity mismatch, since different pulses propagating in the fiber can do so in different modes of dispersion [1].

2.6 Four-wave mixing

Four-wave mixing (FWM) is a nonlinear phenomenon in which at least two optical signals are launched in a nonlinear medium. It results in generation of new optical signals at wavelengths different of the two input signals [18].

If three optical signals are launched into a fiber with frequencies ω_1, ω_2 and ω_3 they will interact with each other and a new signal will emerge at ω_4 that is called idler [3]. For these signals it applies $\omega_1 + \omega_2 = \omega_3 + \omega_4$ [2]. Interaction of these three (four) signals can result in a large number (M) of newly created idlers at differences of frequencies of original signals [3]. We can receive a number of newly created idlers by solving [3]:

$$M = \frac{(N^3 - N^2)}{2} \tag{2.6.1}$$

where N is number of optical signals sent into fiber. If two pump signals are frequency matched ($\omega_1 = \omega_2$) then phenomena is called degenerated four-wave mixing (DFWM) [19].

In case of DFWM where ω_1 and ω_2 are degenerated and $\omega_1 = \omega_2 = \omega_p$ (they have same frequency but different wave vector [18]) then $\omega_3 = \omega_s$ will force pump to give one photon to signal ω_s and one to idler ω_i [3]. As result exchange of energy occurs. Whole situation can be seen in Fig. 2.6.1.

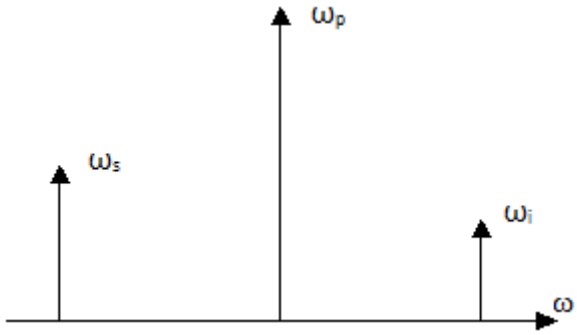

Fig. 2.6.1: Degenerated four-wave mixing

These three signals (waves) can be described by their field intensities as [3]:

$$\mathrm{E}_{(\mathrm{x,y,z})} = \mathrm{f(x,y)}\frac{1}{2}\left[\mathrm{A_p}(z)\exp\left(\mathrm{i}\beta_\mathrm{p}\mathrm{z} - \mathrm{i}\omega_\mathrm{p}\mathrm{t}\right) + A_s(z)\exp(i\beta_s z - i\omega_s t) + A_i(z)\exp(i\beta_i z - i\omega_i t) + c\right] \tag{2.6.2}$$

By applying nonlinear Schrödinger equation to amplitudes $A(z)$ we can receive expressions [3]:

$$\frac{dA_p}{dz} = i\gamma\left[\left(|A_p|^2 + 2(|A_s|^2 + |A_i|^2)\right)A_p + 2A_sA_iA_p^*\exp(i\Delta\beta z)\right] \tag{2.6.3}$$

$$\frac{dA_s}{dz} = i\gamma\left[\left(|A_s|^2 + 2(|A_p|^2 + |A_i|^2)\right)A_s + A_i^*A_p^{2*}\exp(-i\Delta\beta z)\right] \tag{2.6.4}$$

$$\frac{dA_i}{dz} = i\gamma\left[\left(|A_i|^2 + 2(|A_p|^2 + |A_s|^2)\right)A_i + A_s^*A_p^{2*}\exp(-i\Delta\beta z)\right] \tag{2.6.5}$$

Where $A_p(z)$ is amplitude of pump signal, $A_s(z)$ is amplitude of signal at ω_s and $A_s(z)$ is amplitude of signal of created idler. $\gamma = \frac{\omega_p}{c} \cdot \frac{n2}{A_{eff}}$ is nonlinear coefficient as presented in 2.2.2. and $\Delta\beta$ is difference of propagation constants [19]:

$$\Delta\beta = \beta_s + \beta_i - 2\beta_p \tag{2.6.6}$$

2.7 Solitons

Solitons are optical pulses that propagate in nonlinear medium with similar properties as particles. The soliton can propagate in a medium without changing its spectral envelope and can even survive the collisions [2].

The generation of the soliton is a result of balance between spectral broadening of the GVD and pulse compression that occurs in SPM. For pulse compression the chirp caused by SPM has to satisfy the condition of $GVD \cdot C << 0$ [2].

To describe the generation of solitons we can use a nonlinear Schrödinger equation in the presence of GVD and SPM [2]:

$$\frac{\delta A}{\delta z} + \frac{i\beta_2}{2}\frac{\delta^2 A}{\delta t^2} - \frac{\beta_3}{6}\frac{\delta^3 A}{\delta t^2} = i\gamma|A|^2 A - \frac{\alpha}{2}A \tag{2.7.1}$$

Where β_3 is higher order dispersions, α is attenuation of the fiber and the γ represents the nonlinearity coefficient (equation 2.2.2). To simplify the description, we can forgo the attenuation α and higher order dispersion β_3. We can also normalize the equation [2]:

$$\tau = \frac{t}{T_0}, \qquad \xi = \frac{z}{L_D}, \qquad U = \frac{A}{\sqrt{P_0}}$$

where T_0 is the length of the pulse, P_0 is the peak power of the pulse and L_D is dispersion length. After normalization and setting $\beta_3 = 0$ and $\alpha = 0$, we get the equation [2]:

$$i\frac{\delta U}{\delta \xi} - \frac{s}{2}\frac{\delta^2 U}{\delta \tau^2} + N^2|U|^2 U = 0 \tag{2.7.2}$$

where s accounts for the sign of β_2 (i.e. -1 for anomalous dispersion and +1 for normal dispersion) and N^2 is a parameter for pulse and fiber combination. Since the parameter s can achieve both positive and negative values, it is possible to create solitons in both anomalous and normal dispersion.

Solitons with positive β_2 (normal dispersion) are called dark solitons and result in a decrease in power of the background that remains unchanged during propagation [2]. The solitons with negative β_2 (anomalous dispersion) are then called bright solitons and result in pulses that propagate in fiber without changing its envelope.

2.8 Stimulated Raman scattering

The Stimulated Raman scattering (SRS) is a non-elastic scattering that converts wave propagating in a fiber into a wave of lower energy. The difference results in a form of phonon that is absorbed by the molecules of the material. The absorbed energy causes the molecules to be in an excited vibrational state [2].

The scattering of the light then creates a wave that can propagate in co-propagating and counter-propagating direction. The scattered light is then Stokes shifted by up to 13 THz and the spectrum then extends over 10 THz for silica based fibers. The Raman gain spectrum can be seen in Fig. 2.8.1. [21].

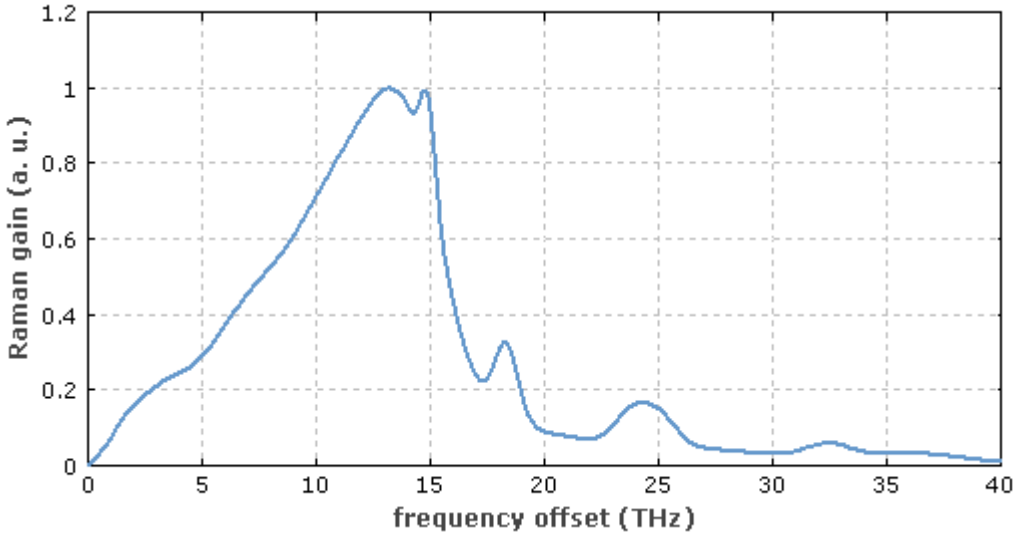

Fig. 2.8.2: Raman gain spectrum for silica fibers [21].

For soft glass fibers PBG 08 (lead-bismuth-gallium-oxide glass) the Raman shift can be up to 30 THz [20]. The amount of Stokes shift is determined by the energy absorbed in material molecules [2]. The shift of scattered light towards longer wavelengths is called Stokes while shift to shorter wavelengths is called anti-Stokes. Both Stokes and anti-Stokes shift can be seen in Fig. 2.8.2.

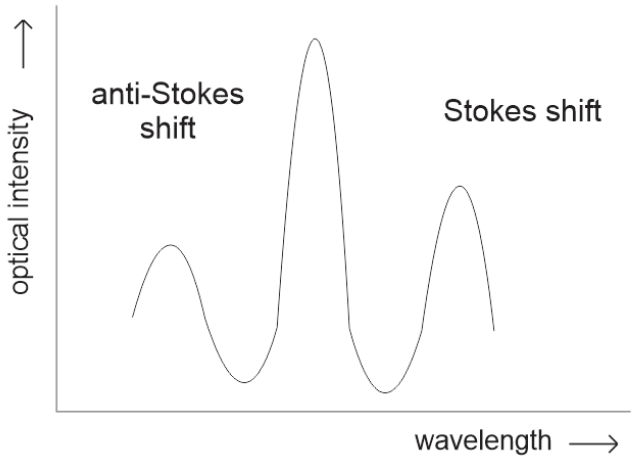

Fig. 2.8.2: Stokes and anti-Stokes shift of the scattered light.

Since it is a stimulated scattering, the SRS can only occur after reaching a threshold level and can be estimated as [2, 3]:

$$P_{th} \approx \frac{16\alpha(\pi w^2)}{g_R} \tag{2.8.1}$$

where g_R is SRS gain, α represents fiber attenuation and w is the spot size that is gained from $A_{eff} = \pi w^2$ (for Gaussian pulse).

The SRS gain depends on the decay time of the excited molecules that is based on the material. In case of glass fibers, the excited molecules merge together into band that causes a broad Raman spectrum [2], as can be seen in Fig. 2.8.2. [21].

2.9 Stimulated Brillouin scattering

The stimulated Brillouin scattering (SBS) is in its nature very similar phenomena as Raman scattering. The difference is that while in Raman scattering the optical phonons create the new co or counter propagating wave, in SBS it is acoustic phonons that are present [2].

SBS converts transmitted light launched into fiber into counter-propagating light wave with Stokes-shift (down shifted) frequency [3, 2, 28]. Frequency downshift is around 10 – 14 GHz [3, 2]. SBS is caused by excited co-propagating acoustic wave due to of nonlinearity caused changes in the material density with applied high optical power. It is a process where material becomes more compressed when electric field is present. Such process is called electrostriction [2].

SBS is dominant optical fiber nonlinearity [28]. Intensity of light scattered through SBS increases exponentially after power threshold needed for SBS to occur is reached [2]. Power threshold is described in [1]:

$$P_{th} = \frac{21kA_{eff}}{g_0 L_{eff}} \left(\frac{\Delta\nu_B + \Delta\nu_P}{\Delta\nu_B}\right) \tag{2.9.1}$$

where *k* is polarization factor between 1 and 2, A_{eff} is effective fiber area, g_0 is Brillouin gain coefficient, L_{eff} is effective interaction length, $\Delta\nu_B$ is Brillouin line width and $\Delta\nu_P$ is pump spectral light.

SBS induces limitation to optical communication systems by reducing maximum usable power. These limitations mainly apply to amplifiers (such as parametric amplifiers or Raman amplifiers) and lasers [28]. High power is also needed for transparent wavelength conversion and efficient phase conjugation [3]. Effects of SBS on signal power can be seen in Fig. 2.9.1 [29]:

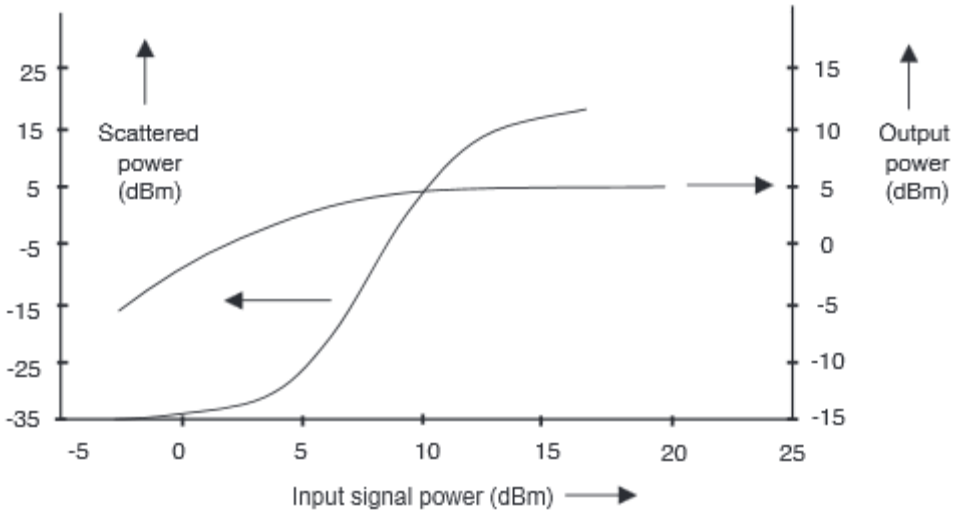

Fig 2.9.1: Effect of SBS on signal power [29].

SBS can be suppressed by broadening spectrum width (which reduces overall power in carrier wave) [28], as can be seen in equation 2.9.1, and such technique is very common [3, 28]. However, such approach is limited by dispersion limitation given by spectrum broadening.

Power threshold is also dependent upon data format – for instance a single pulse with short width would not induce SBS, contrary to a bit stream. Typical value of SBS power threshold is ~5 mW or 7 dBm [2].

3. Properties of Photonic Crystal Fibers

In this chapter I will study the properties of the Photonic Crystal optical fibers. Namely their basic guiding principles, dispersion profiles and how these values can be modified. I will be focusing on the solid-core guiding fibers.

3.1 Basic guiding properties

Photonic crystal fibers are an alternative fiber technology to the classical solid fibers with higher density (and refractive index) core than cladding [4].

These fibers are designed in such a way that they present intentional, periodical defects in the structure of the fiber. These defects are represented in a form of a periodical air-hole structure and that has different refractive index as the rest of the material. Therefore, when an electromagnetic wave propagates in such a medium it leads to the existence of band structure [22].

When light enters the photonic crystal structure, the light can be either reflected or diffracted. The direction of diffracted light depends on the periodicity of the photonic crystal structure and the amount of the diffracted light depends on the distribution of refractive index in the fiber structure [22].

To describe the propagation of electromagnetic wave in photonic crystals we can use Maxwell equations for propagation in a periodic, loss-less media. The results of these equations are again periodic and provide Bloch modes that can be represented in 2D periodic lattice as summation of space harmonics. The resulted wave equation for magnetic field H_k can be seen in 3.1.1. [22, 23] and the periodic lattice is depicted in Fig. 3.1.1.

$$H_k = \sum_G h_G H_0 exp[-i(k-G)r] \tag{3.1.1}$$

where G is lattice vector in periodic lattice, k is wavevector.

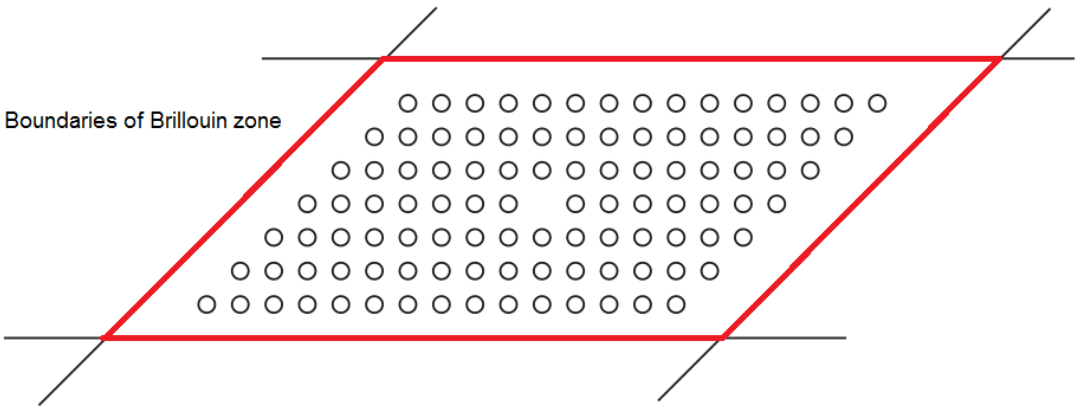

Fig. 3.1.1: 2D periodic PCF lattice containing crystal structure and defects (air holes). Brillouin zone boundaries are marked in red.

Due to the periodical distribution of defects and therefore refractive index, the propagation of the optical wave is also periodical in space of propagation constants (k-space). This

leads to the definition of Brillouin zones as depicted in the Fig. 3.1.1. Brillouin zones boundaries surround the primitive cell in the periodic lattice structure and provide the solution in the form of Bloch waves [22].

Bloch waves are the wavefunctions that provide the solution for periodically repeating environment. Since the propagation of optical wave is also periodical in direction of propagation constant, the solution from a single Brillouin zone is sufficient to describe the periodical medium (PCF) [22].

The construction of PCF as 2D photonic crystal is then based on the planar waveguides and the air holes with low refractive index are used to confine the wave around the solid material core with higher refractive index and thus provide the waveguide [22].

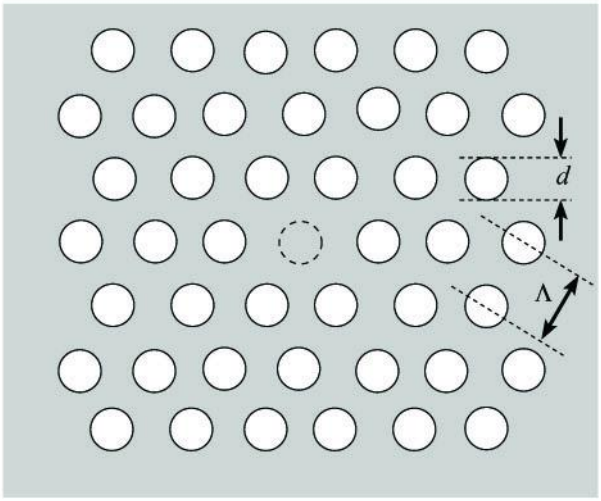

Fig. 3.1.2: Example of 2D periodic PCF structure with air holes' diameter d and distance between air holes Λ [24].

Fig. 3.1.2. [24] depicts a possible PCF structure, with solid core surrounded by periodic, lower refractive index air-holes. For this fiber a photonic bandgap effect phenomenon is used. Photonic bandgap is a mechanism that reflects the light by periodic structure, in this case air holes. It is only possible to reflect the optical waves with wavelength that is equal to twice the period of the air hole structure Λ [4, 22].

This results in guidance of only one fundamental mode, as all the higher modes with smaller or larger wavelengths would pass the air-hole structure unobstructed [4, 22].

The guidance of higher modes is strongly dependent on the structures air-fill factor, that is defined as d/Λ [4, 22, 23]. It has been found out, that the triangular structure PCFs, such as depicted in Fig. 3.1.3 [26, 27], would guide only fundamental mode if the air-fill factor $\sim d/\Lambda < 0.4$ [4, 22, 24]. These fibers are therefore called endlessly single-mode fibers [4]. The situation is depicted in Fig. 3.1.3 [24].

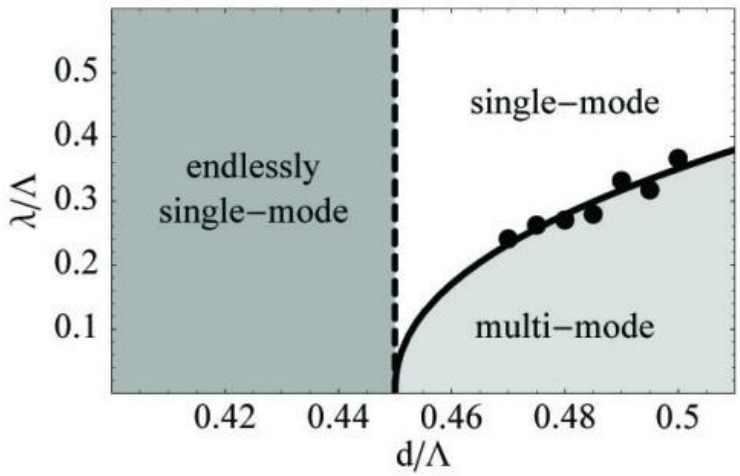

Fig. 3.1.3: Illustration of guided modes in PCF fibers as dependent on the wavelength λ and the air-fill factor $^{d}/_{\Lambda}$ [24].

Examples of the solid core PCFs can be seen in Fig. 3.1.4. [26, 27].

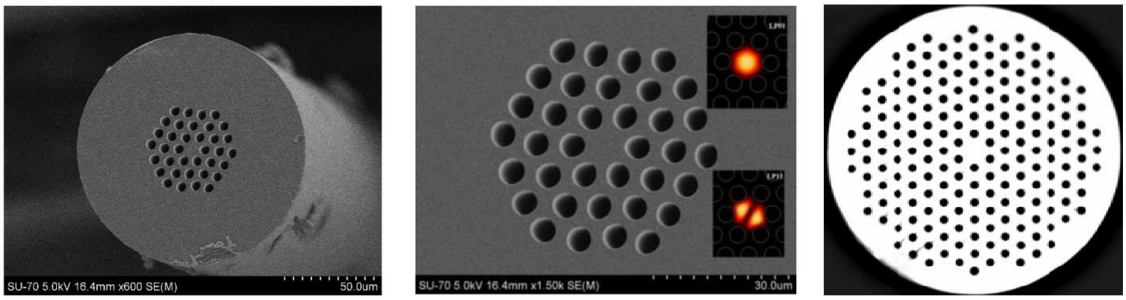

Fig. 3.1.4: Examples of solid core PCFs [26, 27].

The high reflectivity bandgap effect allows for the new approach to fiber design as it is possible to confine and guide a wave even in a low refractive index medium, such as air. Therefore, it is possible to create a fiber with hollow-core that would still guide the light [4, 24], something that is impossible with the use of classical solid fibers. Example of these fibers can be seen in Fig. 3.1.5 [30].

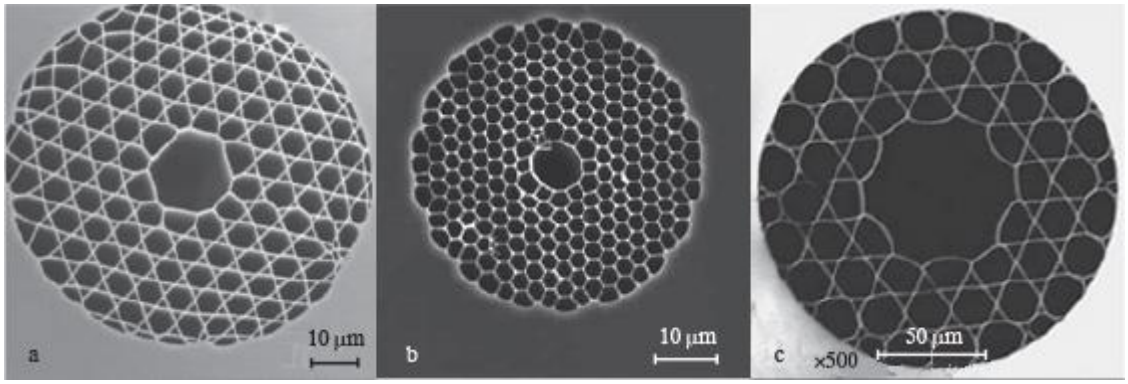

Fig. 3.1.5: Examples of hollow-core fibers PCFs [30].

The important part photonic core fibers is the attenuation they offer. For both hollow-core and solid-core PCFs the losses mechanisms are the same. They are Rayleigh scattering, confinement loss, bending loss and fiber imperfections along the axis. Losses are divided into intrinsic losses and beam confinement or leakage losses [4].

Intrinsic losses can be described by the equation 3.1.2. [4]:

$$\alpha_{dB} = {}^{A}/_{\lambda^4} + B + \alpha_{OH} + \alpha_{IR} \tag{3.1.2}$$

where A is Rayleigh scattering coefficient, B is imperfection loss, α_{OH} is OH absorption loss and α_{IR} is infrared absorption loss. In PCFs the OH absorption losses are the dominant factor with losses over 10 dB/km [4].

Confinement losses are responsible for the leakage of the guided light through the air-hole structure due to finite number of air-holes in the cross section of the PCF and imperfection (irregularities) in this structure. To reduce, or even eliminate, the confinement losses, it is required to design the air-hole structure with large enough air-hole diameter, spacing between air holes and large core area. However, large air-fill factor ${}^{d}/_{\Lambda}$ causes fiber to be multimode [4, 22, 24].

As a result, the PCFs offer higher losses than solid fibers with. However, with the proper design of air-fill factor, core size and control of OH impurities it is possible to achieve attenuation of 0.37 dB/km for solid core fibers and 1.2 dB/km for hollow core [31]. The development of PCFs attenuation can be seen in Fig. 3.1.6. [4].

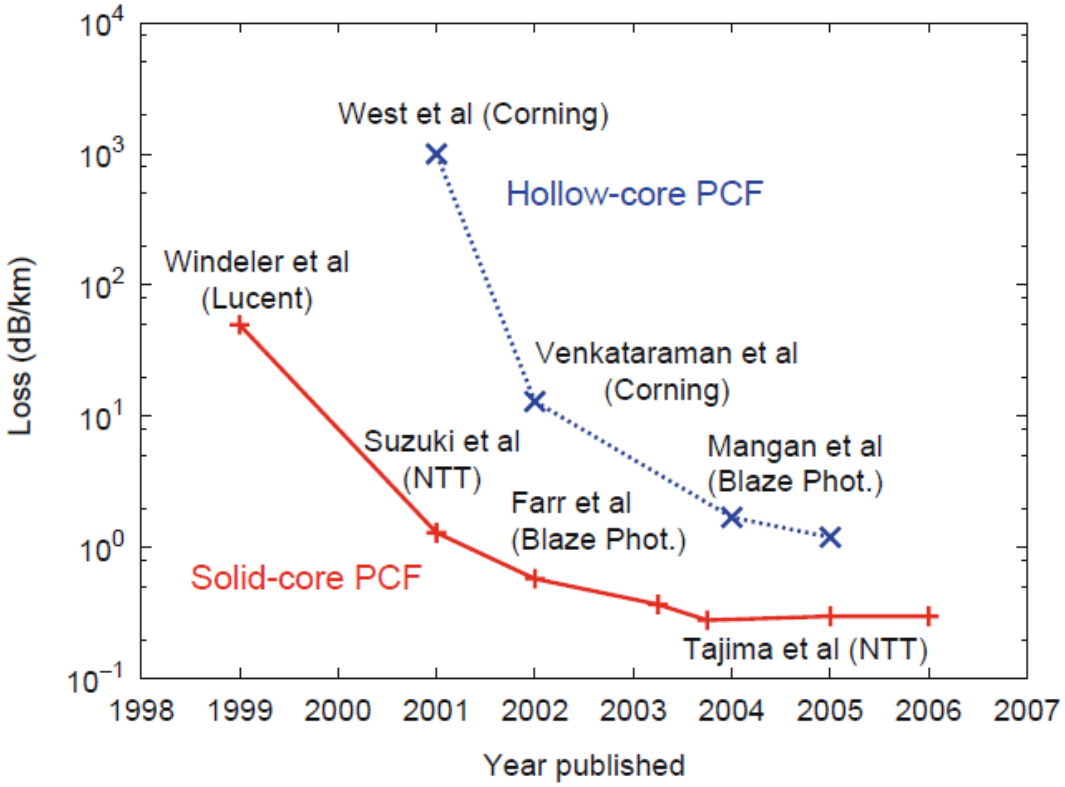

Fig. 3.1.6: Development of attenuation in solid-core and hollow-core PCFs [4].

Advantage of PCF fibers is that their properties can be easily modified to suit the application. The linear part of the refractive index as described in (2.2.1) can be modified using dopants, as can be seen in Fig. 3.1.7 [32]. Where the different concentrations of rare earth ions of Er^{3+} have been used.

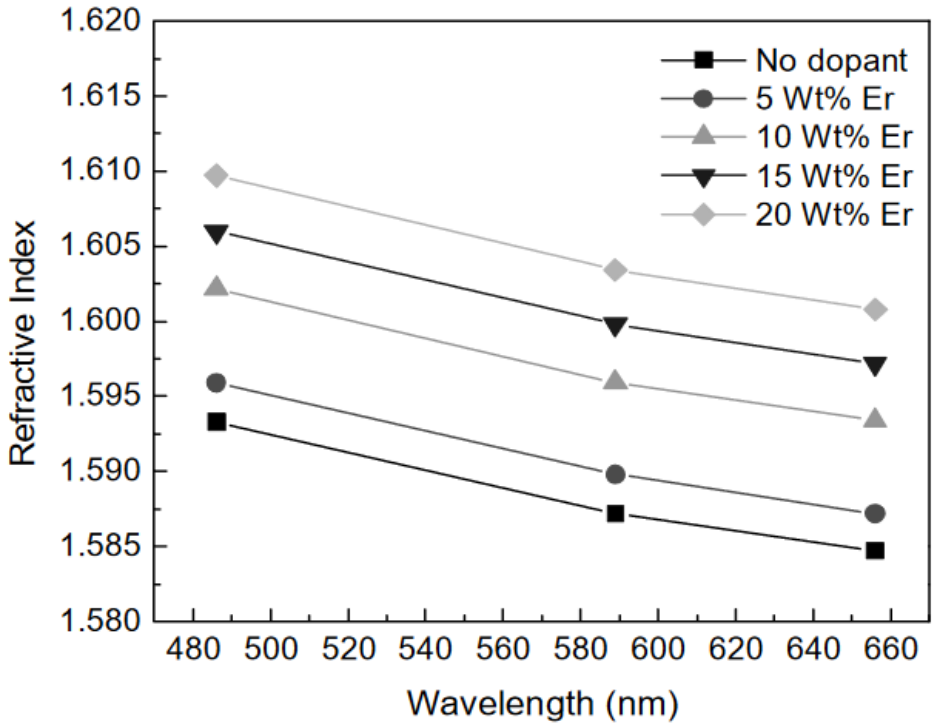

Fig. 3.1.7: Example of refractive index difference using Er^{3+} ions as dopants [32].

The nonlinear part of refractive index n_2 as is described in (2.2.1) can be also changed by introducing dopants. The typical value of n_2 in silica fibers is typically in order of 10^{-20} m^2/W [2, 34]. However, PBG 08 (lead-bismuth-silicate glass) PCF fiber has n_2 value of $4.3x10^{-19}$ m^2/W [33].

The dopants however present a disadvantage, as doping fiber with additional substances presents additional intrinsic losses and the resulted fiber has attenuation in order of dB/m. These dopants can also change the mechanical properties of the fiber and as such it can be fragile.

3.2 Dispersion tailoring

As stated in chapter 2.1 the GVD leads to the pulse broadening and consists of two parts, the material dispersion and waveguide dispersion. For typical single mode fibers, the material dispersion is dominant as it is a solid fiber and the properties of the waveguide are significantly smaller [4, 5].

However, PCFs often have a large air hole structure with much smaller core and thus the design of air-hole structure of PCF contributes significantly to the resulting dispersion, as the structure exhibits strong waveguide properties. Therefore, we need to consider both, the material and waveguide dispersion [5, 35, 36].

The advantage of PCFs is that with the proper design air-hole diameter (d) and the distance between the air-holes (pitch Λ) the dispersion curve can be easily manipulated to shift the ZDW over the large range of wavelengths and the resulting dispersion curve can be flattened or used to compensate anomalous dispersion [4].

To compensate for anomalous dispersion a small core of $d_{core} = 2\Lambda - d$ [4] with large air holes d and small pitch Λ can be used. Example of such solution can be seen in Fig. 3.2.1. [4].

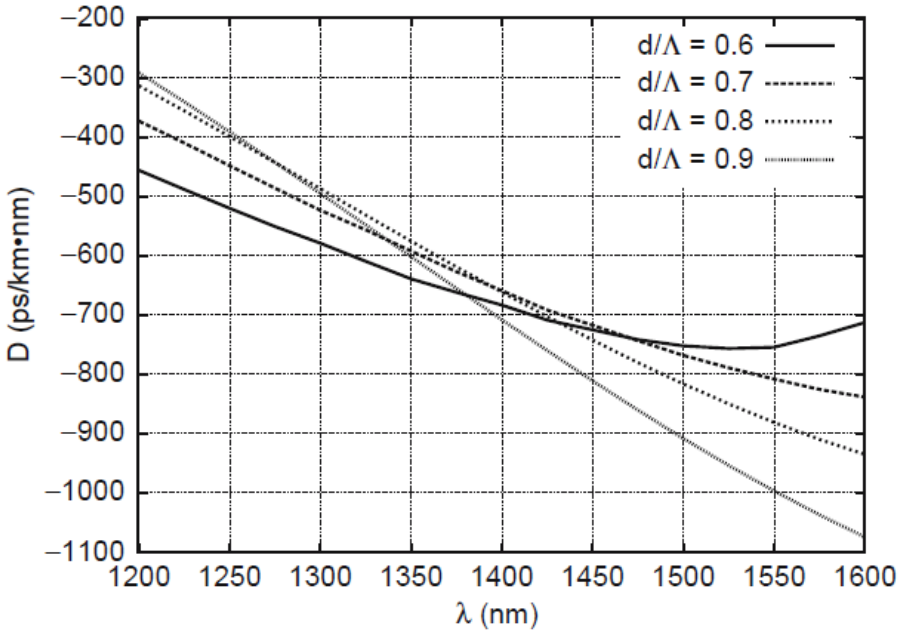

Fig. 3.2.1: Example of dispersion compensating triangular PCFs with pitch Λ = 0.8 [4].

To flatten the dispersion curve it is possible to use two approaches. The first one uses progressively increasing air-hole diameter d in the cross section from the core of the fiber. The situation can be seen in Fig. 3.2.2. [4].

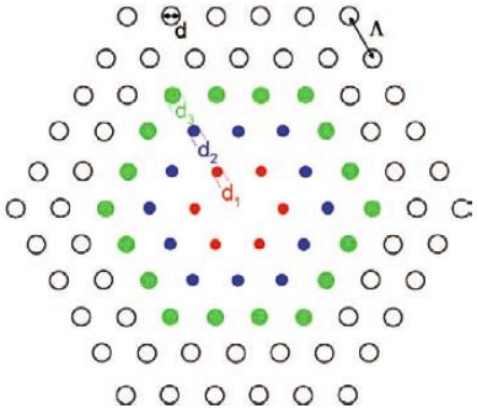

Fig. 3.2.2: Example of PCF fiber designed for flattened dispersion curve with increasing air-hole diameter d [4].

With this approach changing only the first ring has the largest effect on dispersion curve. By decreasing the air-fill factor d/Λ the dispersion value increases and the slope increases (dispersion curve flattens). By modifying the d_2 and d_3 the slope and dispersion value changes similarly however, to the lesser degree. This is caused by tight beam confinement of the fiber [4]. The result of modification of d_1, d_2, and d_3 can be seen in Fig. 3.2.3 [4].

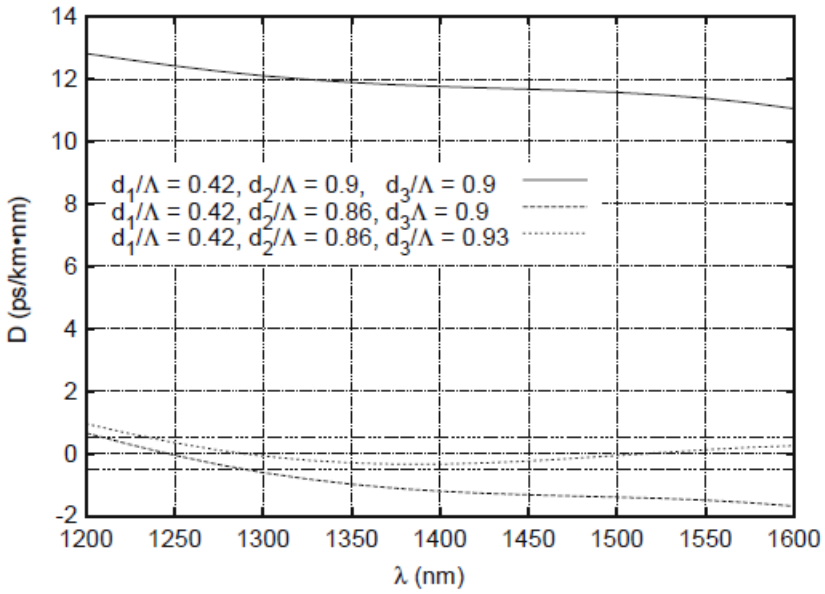

Fig. 3.2.3: Flattened dispersion curve as result of variable modification to the diameter of the air-hole structure [4].

The second method is to use a dopant in the core area of PCF. The first ring of air-holes is modified with three regions of fluorine doped areas and the central core area is doped with germanium [4, 37]. The situation can be seen in Fig. 3.2.4. [4].

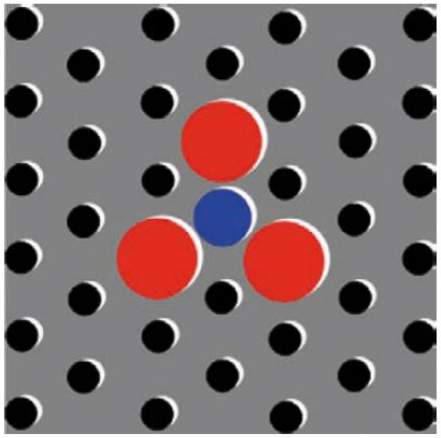

Fig. 3.2.4: Schematics of doped PCF with fluorine doped area marked in red and germanium doped core marked in blue [4].

This approach allows for further control in the shaping of the dispersion curve. Where by changing the diameter of the fluorine doped areas d_f it is possible to shift the ZDW and by further optimizing the pitch Λ and air-fill factor d/Λ, it is possible to achieve a flattened dispersion curve as can be seen in Fig. 3.2.5. [4].

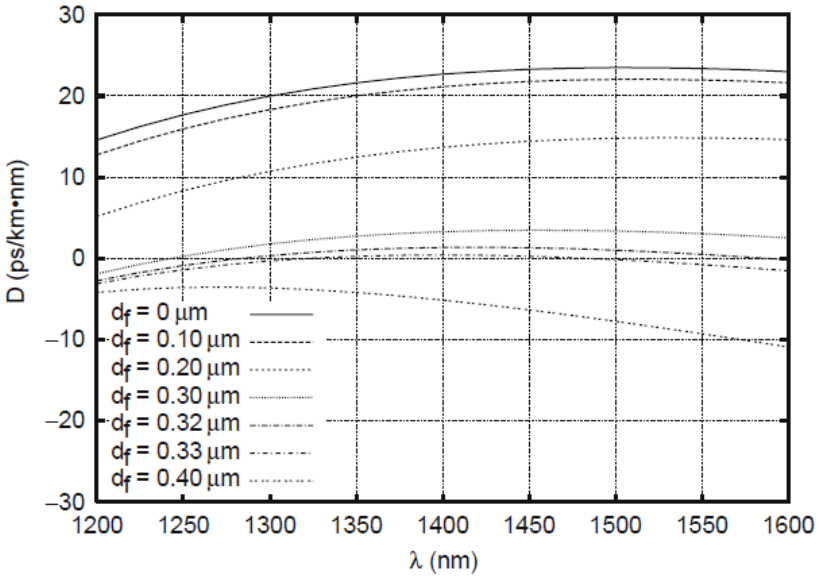

Fig. 3.2.5: Flattened dispersion curve as a result of doped core area PCFs with d = 0.65, Λ = 1.7 μm and d_f as a function of dopant area diameter [4].

3.3 Nonlinearity

Nonlinearity or the Kerr effect and the nonlinearity coefficient *γ* have been described in chapter 2.2. From the equation 2.2.2 it is apparent that the nonlinearity is highly dependent on the effective area of the fiber and nonlinear refractive index n_2 that in turn is dependent on the optical intensity of the wave propagating in a fiber.

The PCFs offer a high nonlinearity through high confinement of the propagating wave in a small core size fiber. Moreover, PCF fibers can be manufactured from different, non-silica materials such as bismuth, chalcogenide, sapphire, gallium or lead, with higher nonlinear refractive index n_2 [37, 38]. These materials also provide higher transparency in the longer wavelengths, as opposed to silica based fibers [37].

Properly designing of the air-hole structure of the PCF cross section can be used to tailor the nonlinear refractive index coefficient n_2. This requires the modification of the air-fill ratio d/Λ, air-hole diameter d and the pitch Λ. The result of such tailoring can be seen in Fig. 3.3.1. [36].

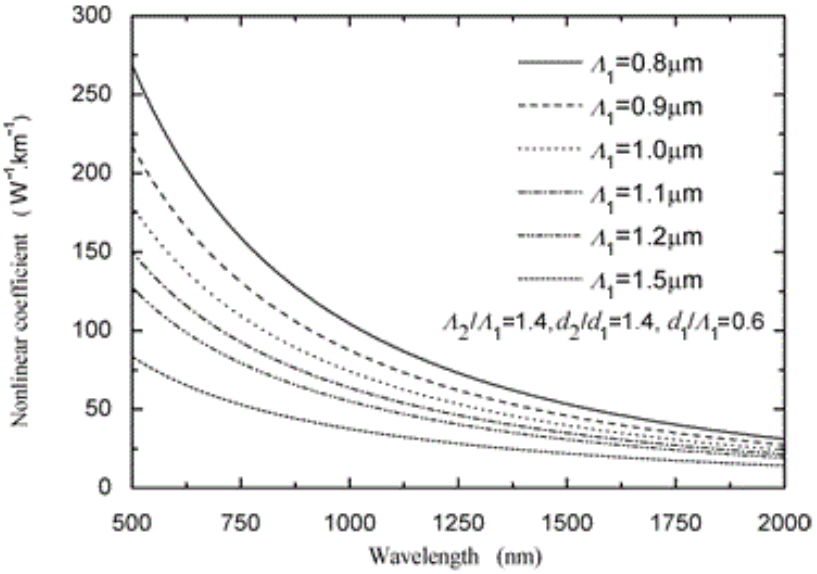

Fig. 3.3.1: Example of nonlinear refractive index coefficient tailoring by changing the pitch Λ, air-hole diameter d and air-fill ratio d/Λ [36].

In the Fig. 3.3.1. it can be observed that with the decreasing pitch Λ_1 of inner air-hole ring the nonlinear refractive index coefficient n_2 increases.

In addition, the doping of the core as described in section 3.2. can be used to achieve both, high nonlinearity γ and the flat dispersion curve. Using for example chalcogenide core tellurite cladding with core diameter d_{core} = 0.625 μm high nonlinearity of γ = 31 $W^{-1}m^{-1}$ at 800 nm or 11$W^{-1}m^{-1}$ at 1550 nm while still maintaining flat dispersion curve [38]. This is caused by very small effective area of the fiber. The situation can be seen in Fig. 3.3.2. and 3.3.3. [38].

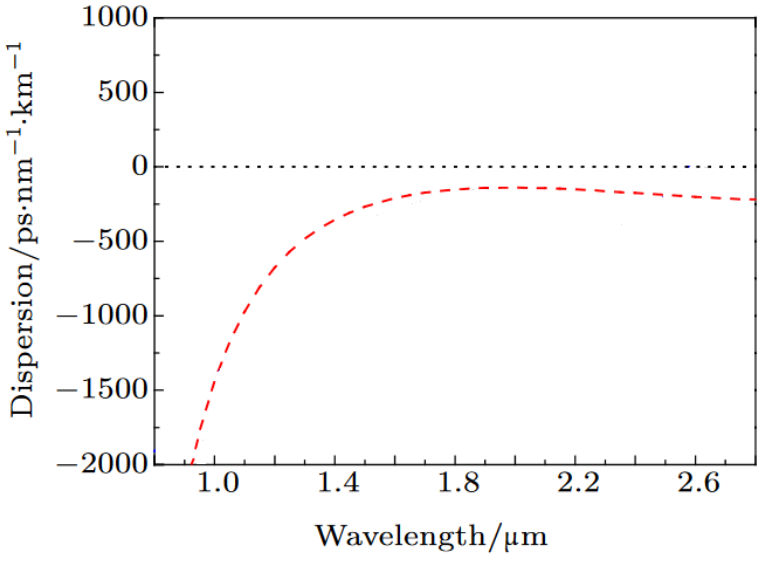

Fig. 3.3.2: Flat dispersion curve of chalcogenide core tellurite cladding PCF with d_{core} = 0.625 μm core diameter [38].

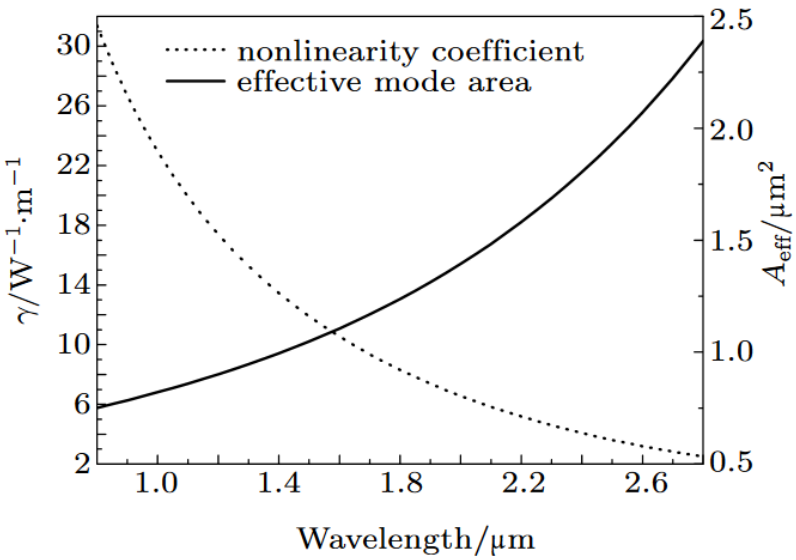

Fig. 3.3.3: Resulting dispersion and effective area of the chalcogenide core tellurite cladding PCF with d_{core}= 0.625 μm core diameter [38].

4. Supercontinuum generation and its conditions

In this chapter I will study the phenomena discussed in chapter 2 as well as their interaction with each other and their effect on generation of the supercontinuum. I will focus on generation of supercontinuum with femtosecond pulse laser (FSL) used as pump.

4.1 Nonlinear propagation and SC generation

Supercontinuum generation is a process that involves the interaction of many nonlinear effects that has been discussed in chapter 2 and leads to the broadening of the initial spectrum. Each phenomenon on itself cannot fully describe the resulting spectrum. It is their interaction that matters.

To describe the nonlinear propagation in the medium along the *z* axis a generalized nonlinear Schrödinger equation (GNLSE) is used [1, 39, 40].

$$\frac{\delta A(z,T)}{\delta z} = \sum_{n\geq 2} \frac{i^{n+1}}{n!}\beta_n \frac{\delta^n A}{\delta T^n} + i\left(\gamma_0 + i\gamma_1 \frac{\delta}{\delta T} - \frac{\gamma_2}{2}\frac{\delta^2}{\delta T^2}\right)\left(A(z,T)\int_{-\infty}^{T} R(T')|A(z,T-T')|^2 dT'\right) \quad (4.1.1)$$

where $A(z,T)$ is optical field envelope, T is time, β_n is the nth derivative of propagation constant, γ_n is nth derivative of nonlinear coefficient.

In supercontinuum generation we can consider only the spectrum broadening caused by chromatic dispersion. However due to the use of the PCF fibers it is important to consider both, the waveguide and material dispersion as they offer strong waveguide effect [1, 4, 5].

For dispersion it is also important to consider the phase velocity and group velocity of the propagating signal. The phase mismatch will limit the interaction of the optical field present in the fiber and plays an important role in frequency conversion process. The group velocity mismatch then influences the interaction length [1].

Self-phase and cross phase modulation plays a role in the ZDW region as only the nonlinearity presented by Kerr effect will take place. It creates a time dependent intensity modulation that results in differences in a local refractive index. The change in refractive index then causes the time dependent phase delay resulting in a nonlinear pulse chirp with generation of the new spectral components [1].

In interaction of SPM and dispersion we can get two modes of operation. The first one leading to both spectral and temporal broadening of the pulse in the normal dispersion region. The second one in anomalous dispersion region leading to the creation of solitons [1].

The generation of the soliton is a result of the balance between spectral broadening of the GVD and pulse compression that occur due to SPM [1, 2]. The soliton propagation equation has been presented in 2.5.2 where N^2 is the pulse and fiber parameter. For the fundamental soliton the $N = 1$ and for the higher order soliton $N \geq 2$. The higher order solitons then undergo a periodic spectral and temporal change [1].

For supercontinuum generation the higher order solitons with $N >> 1$ are considered. Their initial formation in anomalous dispersion region will consist of the spectral broadening. However higher order solitons are unstable and can easily dissolve into several pulses with lower amplitude. This process is called soliton fission and in combination with Raman scattering has the most significant influence in supercontinuum generation with femtosecond

pump lasers [1, 40]. The evolution of one soliton fission into two solitons can be seen in Fig. 4.1.1. [41]

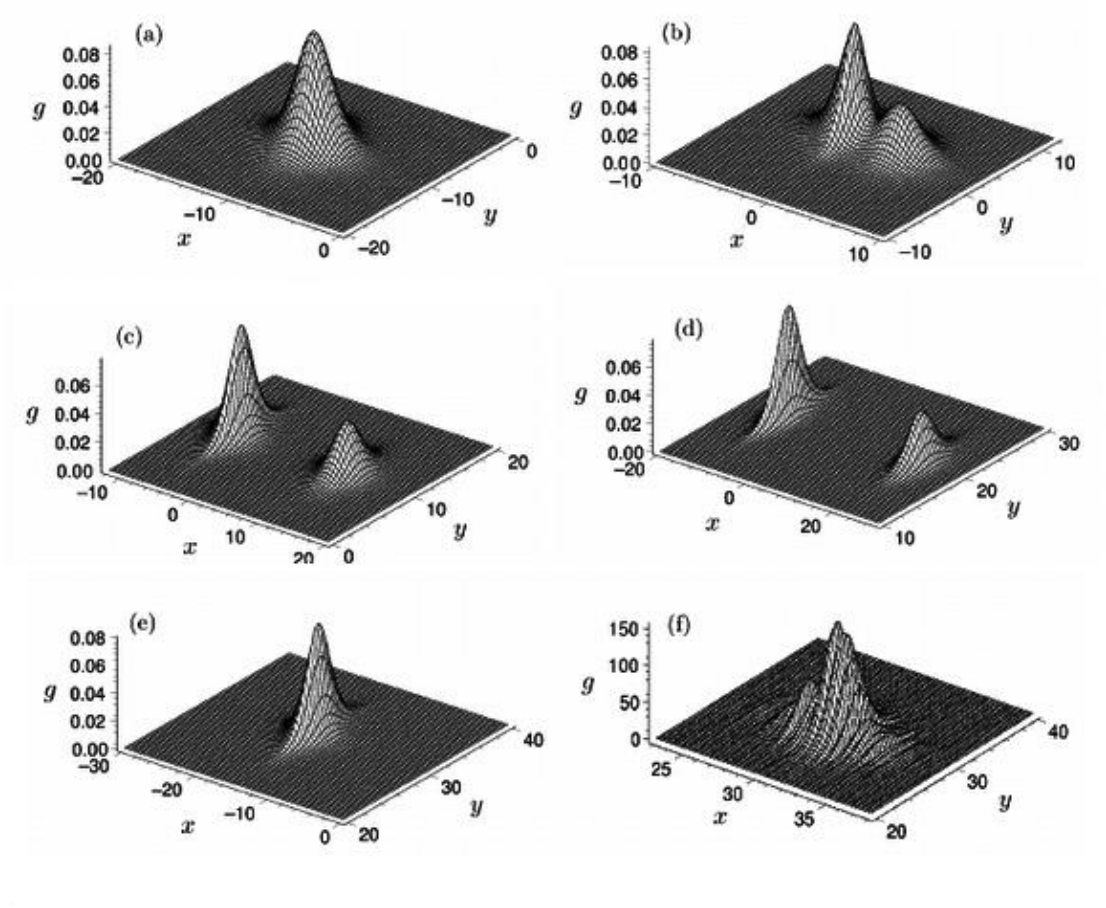

Fig. 4.1.1: The evolution of one soliton fission into two solitons [41].

In case of picosecond and up to continuous wave pump sources. The four-way mixing is a dominant effect on the spectral broadening. As the pump signal is converted into series of sideband that then undergo the spectral broadening [1].

4.2 Supercontinuum generation with femtosecond pulses

In case of a femtosecond pump it is important to consider SRS and the soliton fission as the two main effects. These phenomena have the largest impact on SCG in the long wavelength region after the initial formation of the soliton.

The broadening of the pulse caused by the SPM and its appropriate frequency chirp is then compensated by the compression in anomalous dispersion region thus forming a soliton [1].

The first part of spectrum broadening can be achieved by soliton‘s continuous self-frequency shift. That is caused by the soliton fission and breakup of the initial pulse into many soliton pulses. Each of the solitons induces Raman scattering and appropriate Raman shift and thus generating new spectral components in the longer wavelength region. The Raman frequency shift is possible due to the overlap of the soliton pulses with Raman spectrum gain in the anomalous dispersion region [1].

Further spectral components can then be generated through a dispersive wave. Dispersive wave is generated when the soliton pulse is injected near the ZDW region and the propagating soliton can then transfer a portion of its energy as a dispersive wave in the normal dispersion region [1].

The shift to the lower wavelengths is then governed by interaction of soliton and the dispersive wave through the Raman scattering. In such case a higher order dispersion β_3 is important. The soliton formation and dispersive wave radiation can e seen in Fig. 4.2.1. [4].

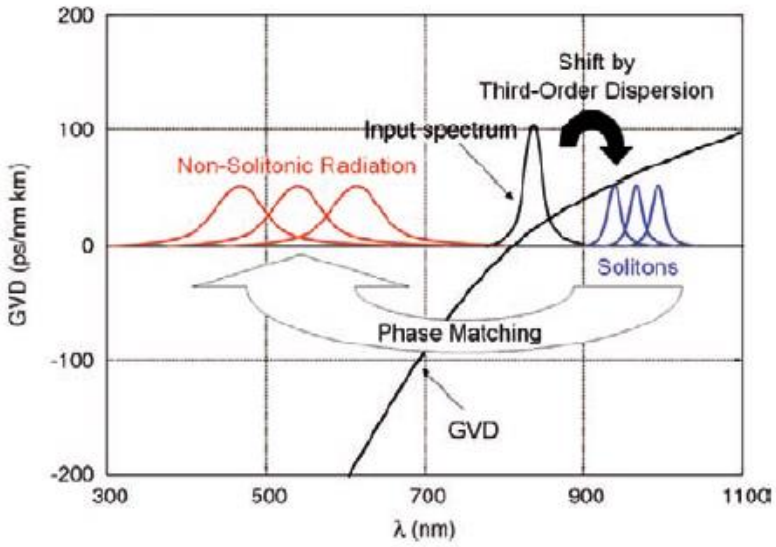

Fig. 4.2.1: Formation of soliton and dispersive wave radiation in regard to dispersion curve.

If $\beta_3 > 0$, the newly created dispersive wave has smaller group velocity then the original soliton. The soliton propagation is however continuously slowed by the Raman effect and the dispersive wave is able to catch up. When that happens the soliton reflects the dispersive wave backwards and the process can repeat again [1].

The generation of the new spectral components at the lower wavelengths is dependent on the group velocity and group index where the group index has to increase with wavelength. Since the group index increases with wavelength the backward reflection results in the shift to the lower wavelengths [1].

For $\beta_3 < 0$ the radiation and dispersive wave is amplified with the distance of propagation. In such case the newly created dispersive wave is created ahead of the soliton and therefore cannot be reflected backwards or interact at all as in case of $\beta_3 > 0$. However, fibers with several ZDW regions exist and the emitted dispersive wave can interact with a different soliton [1].

It is also important to note that the pulse broadening reaches its maximum at certain distance of propagation that is dependent on the soliton fission. This length is therefore called a fission length and can be approximated as [1]:

$$L_{fiss} \approx \frac{L_D}{N} \tag{4.2.1}$$

Where L_D is characteristic dispersive length and corresponds to the soliton order. Both of these can be expressed as [1]:

$$N^2 = \frac{L_D}{L_{NL}}, \qquad L_D = \frac{T_0^2}{|\beta_2|}, \qquad L_{NL} = \frac{1}{\gamma P_0}$$

Where L_{NL} is characteristic nonlinear length, N^2 is parameter for pulse and fiber combination, P_0 is peak power and T_0 is pulse width.

4.3 Conclusion and the conditions for supercontinuum generation

Some of the conditions for the supercontinuum generation have already been described in the previous chapter. For one it is important to use pump laser in the anomalous dispersion region close to the ZDW. In this case we can generate solitons and make use of their fission to frequency shift the newly created solitons to the longer wavelengths as well as use dispersive wave to generate new spectral components at the shorter wavelengths.

To generate solitons, we would require the interaction of correct SPM frequency chirp with GVD. SPM would then be dependent on the high nonlinearity of the fiber.

It is also apparent that the dispersion profile plays the key role in supercontinuum generation and should be as flat as possible in both anomalous and normal region as well as having higher order dispersion β_3 greater than zero.

We can also make use of the fibers with multiple ZDW where β_3 could be negative and we would still be able to generate new spectral components in the shorter wavelength region.

Since all these effects interact with Raman scattering and the initial soliton creation as well as further propagation requires sufficient pump power. It is important to introduce a high enough pump power to reach the Raman scattering threshold. It is estimated around 1 W region.

All of these conditions are best satisfied with PCFs as they allow small core with high power density. Because of the small effective area, we also get high nonlinearity. With rearranging of the air-hole structure and material dopants we can then easily tailor fiber dispersion profile to our needs.

5. Simulation results of supercontinuum generation

In this chapter I will model two available PCFs using COMSOL Multiphysics 5.0 software. I will then estimate the dispersion curve and higher order dispersion constants. Afterwards, using Matlab software I will simulate SCG.

5.1 Fiber modeling and SCG

In this thesis I will study two available PCFs. The first one is marked as NL24C4 and the second one NL29A6. Both of these fibers are manufactured from PBG - 08 glass (lead-bismuth-gallium-oxide glass). First it is required to model the PCF cross-section and provide refractive index of the material as is described by Sellmeier equation. For PBG 08 the Sellmeier equation was measured and provided by VŠCHT as is depicted in Fig. 5.1.1.

For NL24C4 the pitch Λ = 2.39 μm, air-hole diameter d = 1.15 μm and core diameter d_{core} = 3.52 μm. For fiber NL29A6 the pitch Λ = 2.2 μm, air-hole diameter d = 2.1 μm and core diameter d_{core} = 1.8 μm.

$$1.8793 + ((2.672 * 10^4) * (\lambda^{-2})) - ((1.716 * 10^9) * (\lambda^{-4})) \quad (5.1.1)$$

The resulted designed PCFs can be seen in Fig. 5.1.1.

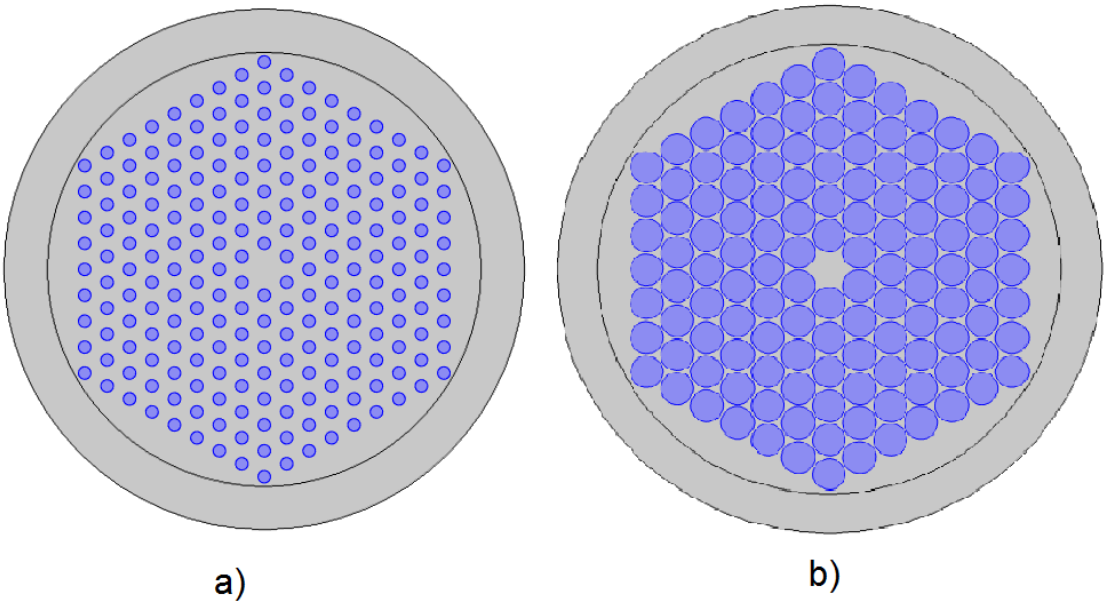

Fig. 5.1.1: Designed PCFs NL24C4 (a) and NL29A6 (b). Blue parts are air-holes with refractive index of air, grey parts represent PBG-08 glass material with refractive index provided by equation (5.1.1).

As is depicted in Fig. 5.1.1. the biggest difference between these fibers is their air-hole diameter d and their pitch Λ. These differences relate in significantly different effective indexes n_{eff} and dispersion curves, as can be seen in Fig. 5.1.2.

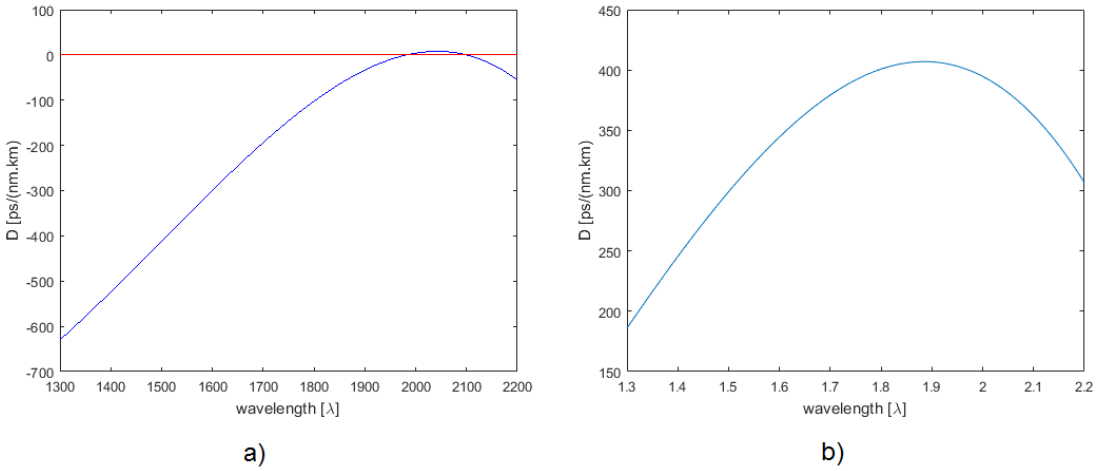

Fig. 5.1.2: Dispersion curves for PCFs NL24C4 (a) and NL29A6 (b).

From the dispersion curve it is then possible to calculate GVD and higher order dispersion values up to β_{10}, these parameters are required for calculation of SCG. For this thesis I used a laboratory build FSL with 1.5 ps pulse duration and 167 W pulse peak power at 1560 nm. This pulse can be amplified using an Erbium-Doped Fiber Amplifier (EDFA), which theoretically provides peak power amplification up to 16.7 kW (at an average output power of 30 dBm). The nonlinear coefficient γ=206.84 $W^{-1}km^{-1}$ for NL24C4 and γ=747.8 $W^{-1}m^{-1}$ for NL29A6.

For SCG I then used Matlab script provided by Dudley et. al, RMP 78 1135 (2006). The resulted SC spectra can be seen in Fig. 5.1.3 and 5.1.4.

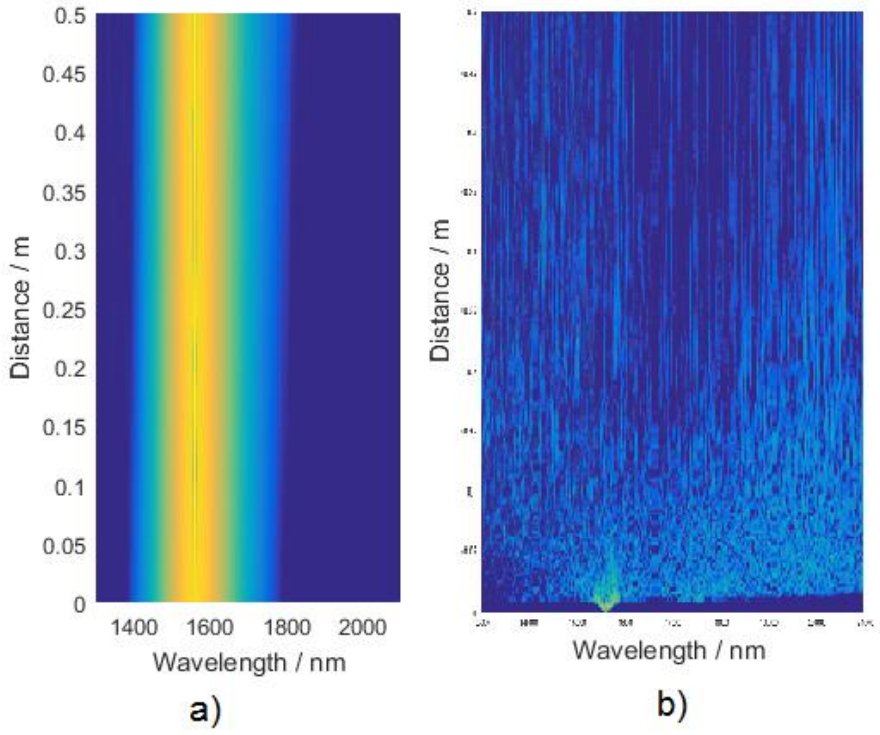

Fig. 5.1.3: Results of simulation of NL24C4 (a) and NL29A6 (b) with 16. 7 kW pulse power (30 dBm EDFA output) for wavelength span of 1300 – 2100 nm with 0.5m long fiber.

In figure 5.1.3 it can be seen, the optimal SCG for maximum of 30 dBm input power, that would showcase best possible result. This input power however, can only be reached by using EDFA amplifier, as FSL offers only 167 W peak power. For NL29A6 the formation of SC can be observed even without EDFA amplification, as depicted in Fig. 5.1.4. (a).

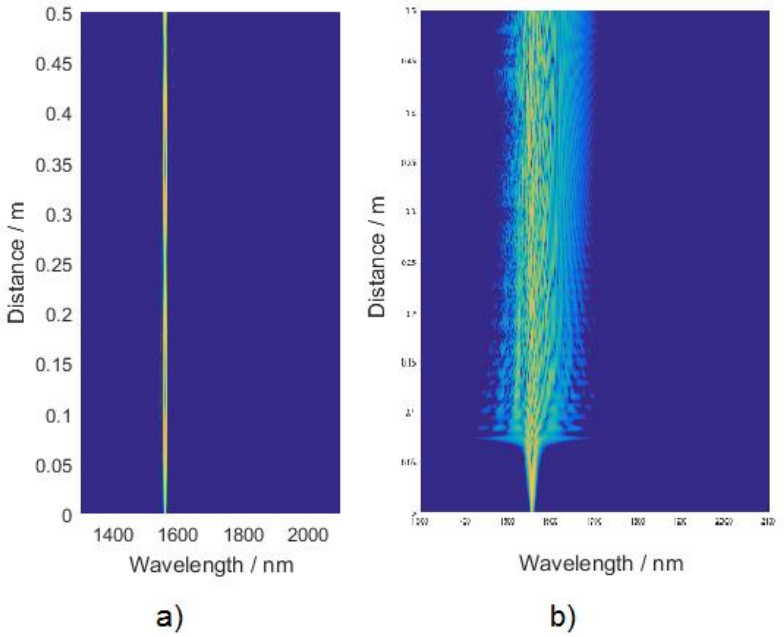

Fig. 5.1.4: Results of simulation of NL24C4 (a) and NL29A6 (b) with 166 W pulse peak power for wavelength span of 1300 – 2100 nm with 0.5m long fiber.

Fiber NL24C4 on other hand requires at least 25 dBm average power input (depicted in Fig. 5.1.4. (b)) for any spectral broadening to occur. This is further reinforced by the fact that NL24C4 offers significantly smaller γ, than fiber NL29A6. However, even when increasing input power by 3 dBm spectral broadening increases only by ~100 nm, as depicted in fig 5.1.5.

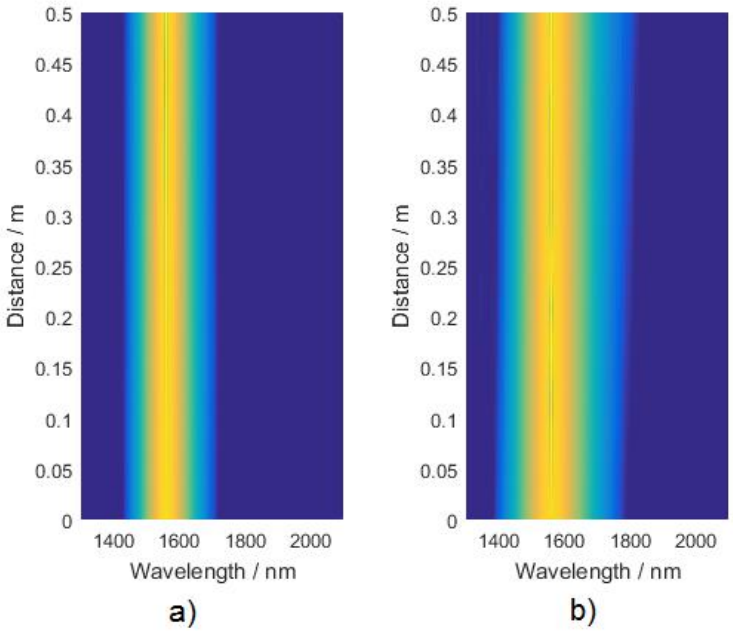

Fig. 5.1.5: Results of simulation of NL24C4 with 5 kW (a) and 10 kW (b) pulse power for wavelength span of 1300 – 2100 nm with 0.5m long fiber.

6. Experimental campaign

In this chapter I will describe the measurement setup and the challenges associated as well as femtosecond pulse generation and the results gained through measurements.

6.1 Femtosecond pulse generation

One of the base components for SC generation is FSL. I use the setup that is based on the nonlinear polarization rotation. A phenomenon, that changes the polarization direction based on the intensity of optical pulse already propagating in the fiber [42].

Since even SMF allows two polarization states to propagate in the fiber, there is a birefringence – a difference in refractive indexes in *x* and *y* axis of the fiber. If there is a high optical signal present in a fiber, the nonlinearity will also influence the nonlinear polarization rotation [42, 43, 44]. This can be understood by the coupled NLSE for *x* and *y* axis of the fiber [43, 44]:

$$\frac{\delta A_X}{\delta z} + \frac{\alpha}{2} A_X = i\gamma\left(|A_X|^2 + 2{A_Y}^2\right)A_X \tag{6.1.1}$$

$$\frac{\delta A_Y}{\delta z} + \frac{\alpha}{2} A_Y = i\gamma\left(|A_Y|^2 + 2{A_X}^2\right)A_Y \tag{6.1.2}$$

where A_X and A_Y are the envelopes of optical field propagating along the axis, α is attenuation coefficient and γ is nonlinearity of the fiber. By solving these equations, a nonlinear phase shift is gained [44]:

$$\Delta\Phi_{NL} = ({}^{\gamma P L_{eff}}/_{3}) \cos\theta \tag{6.1.3}$$

where θ denotes angle between x and y axis of polarization, *P* is the optical power and L_{eff} is effective length of the fiber. As a result, once the pulse passes the isolator, it is linearly polarized, but through the propagation of the optical signal in the fiber, the polarization in *x* and *y* axis changes based on intensity of the signal [44].

The polarization is then again corrected by the PC in such a way, that the signal is linearly polarized in the middle of the pulse, but the edges are not. The signal will then pass through isolator that will permit the signal with linear polarization, but will absorb the edges and thus shorten the pulse.

In this thesis I used laboratory-built FSL that only required the optimization of the output power ratio coupler, but was otherwise finished. The schematics of the FSL can be seen in Fig. 6.1.1.

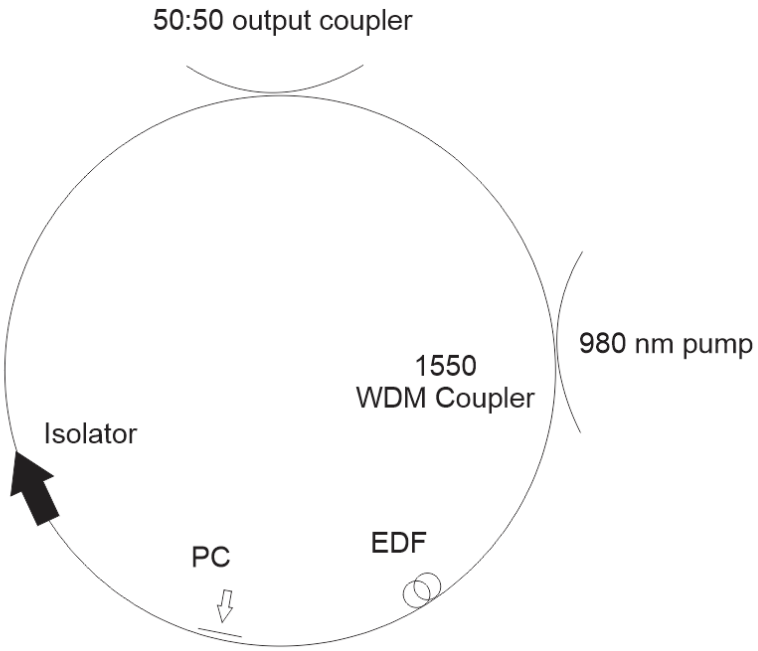

Fig. 6.1.1: Schematics of self – build FSL.

In my setup I generate the femtosecond pulses by pumping Erbium-doped fiber (EDF) at 980 nm with the output of EDF connected as input in a loop. The output of the EDF is connected to the isolator to ensure the propagation in only one direction and to linearly polarize the optical signal. The polarization controller (PC) is then used to match the polarization of the optical signal already propagating in the loop with the one generated in the EDF

In this setup the output of the FSL is coupled by 50:50 coupler, as it was experimentally found that it offers highest FSL output. Since it is important to have enough energy circulating in a loop to ensure the pulsed regime. The current of the EDF pump diode was set to 250 mA. This way I was able to achieve pulse generation of 1.5 ps, peak power of 167 W and 40 MHz at 1560 nm. The spectrum of the output of FSL can be seen in Fig. 6.1.2.

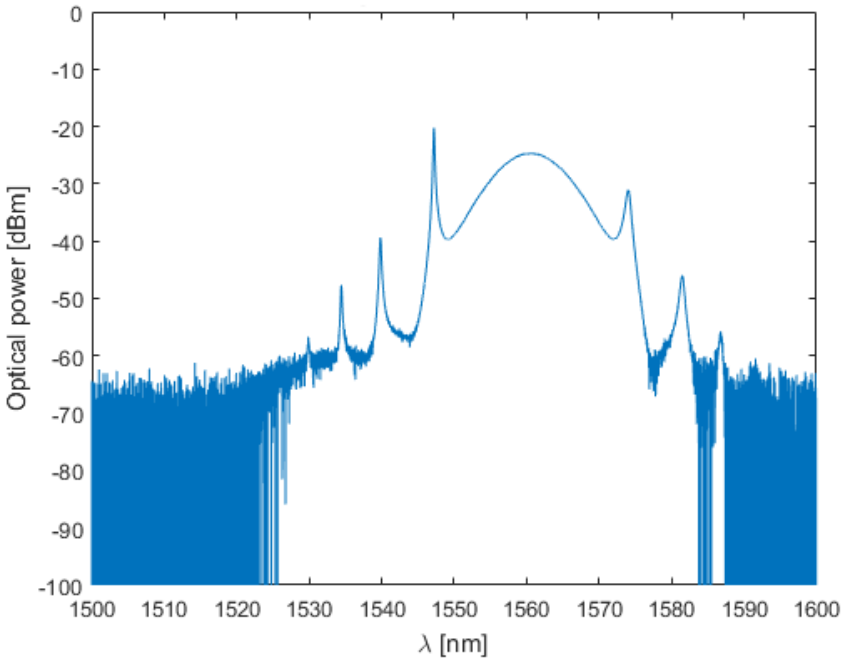

Fig. 6.1.2: Spectrum of FSL.

6.2 Coupling of Photonic Crystal Fibers

As described in chapter 3. and 4. PCFs offer high nonlinearity and flat dispersion curve, therefore I use them in my SCG setup. These fibers have often very small core diameter in order of 1 – 3 μm and as such it is challenging to effectively launch a signal into them. However, PCFs I use have large numerical aperture (*NA*) in order of 0.8 at 1550 nm [45] as opposed to *NA* = 0.14 for SMF-28.

High NA allows for easy of coupling optical signal launched into the fiber, on the other hand it creates significant challenges with coupling the output of the PCF to display the result on the optical spectrum analyzer (OSA). As the signal leaving PCF is launched with an angle of 53º in case of 0.8 NA and needs to coupled into SMF under 8 º.

For the SCG, it is more important to get the highest possible amount of optical power into PCF, as it will contribute to the SCG. The high PCF to SMF coupling loss of up to 25 dB is then secondary, as it is only used to display the results.

However, it is still important to use OSA with sufficient dynamic range to be able to display results and sensitivity better than -50 dBm. For the coupling itself I used the setup that can be seen in Fig. 6.2.1.

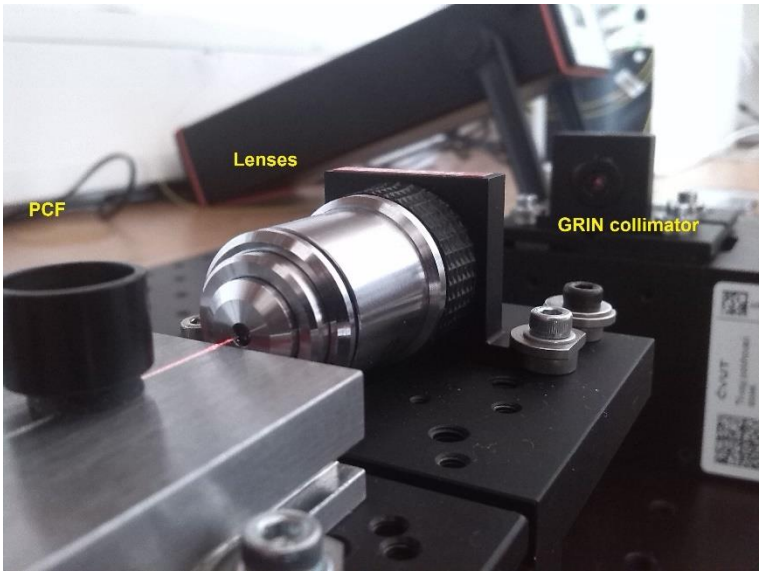

Fig 6.2.1: Coupling setup using lenses.

As it is depicted in Fig. 6.2.1 I used pigtailed Graded-Index (GRIN) fiber optic collimator that launches the signal into PCF through 60x lenses. In this case both PCF and GRIN collimator are positioned on the 3-axis flexure stages while the lenses have fixed position. This allow for fine tuning of the position of both PCF and the GRIN collimator.

The coupling is then done by a visible light laser (VLL) to achieve the initial coupling. I then substituted VLL for tunable laser at 1550 nm and adjusted the setup using the power measured at the output of the PCF. To measure optical power I used Thorlabs PM100D power meter, which has a large and easily positioned photodetector that I position at the unconnected output of the PCF.

This way it is possible to achieve up to 3 dB loss coupling. For improved stability it is useful to use an optical table, but the ordinary table can work as well with measured difference in loss of up to 0.5 dB.

Similar setup can also work for coupling the output of the PCF into GRIN collimator, however the coupling losses can reach up to 26 dB. This is caused by an angle of the beam launched from PCF. Since I have only 3-axis stage available, there is no way to compensate for the angle of the PCF or the GRIN collimator, as is depicted in Fig. 6.2.2.

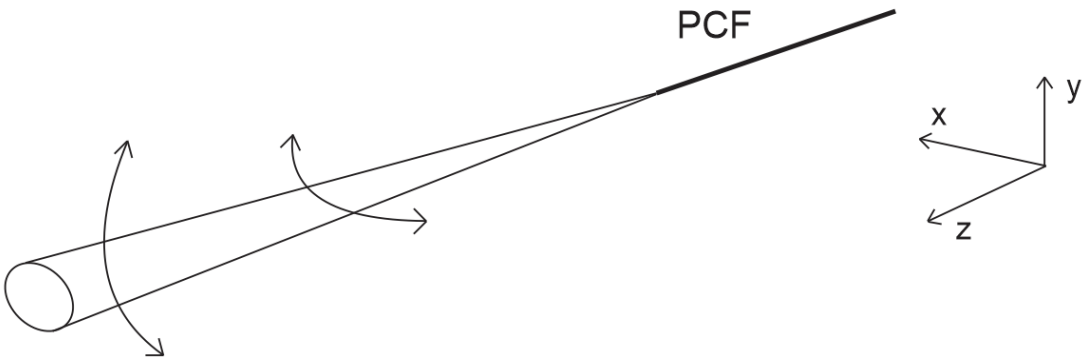

Fig. 6.2.2: Angular error when launching optical signal from PCF.

This results in the maximum of 18 dB coupling loss. This is not a problem if I couple signal into PCF as the signal is launched from small *NA* of 0.14 into high *NA* of 0.8, however in case of coupling out of PCF it is reversed.

For this measurement of SCG I used OSA Yokogawa AQ6370C with 73 dB dynamic range at -10 dBm reference that allowed to display measurement results.

This setup is also affected by maximum optical power limitation imposed by the GRIN collimator. Its datasheet value is 300 mW (24.8 dBm). As a solution, I used the alternative setup. The modified setup can be seen in Fig. 6.2.3.

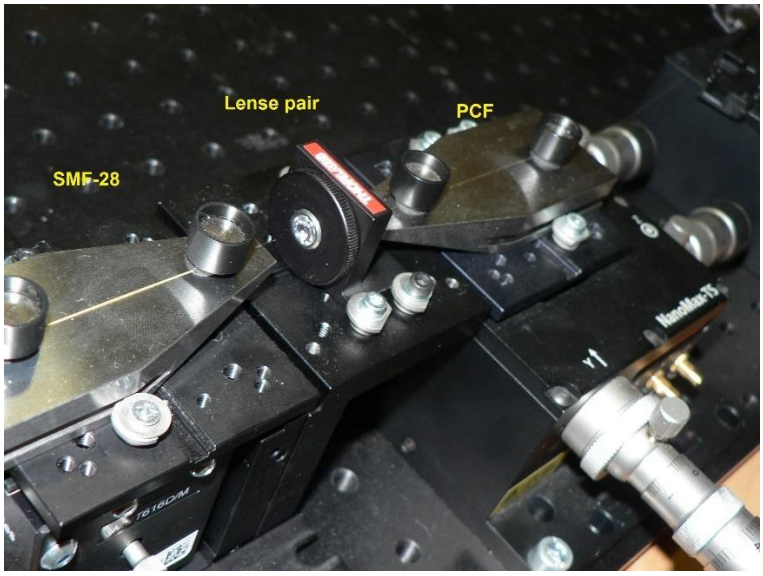

Fig. 6.2.3: Coupling using aspheric lens pair.

Instead of lenses I use mounted aspheric lens pair and instead of GRIN collimator I use spliced SMF, since the lens pair is specifically designed for *NA* of SMF (*NA* = 0.14). Similarly, as in previous setup, both SMF and PCF are placed on 3-axis stage with lens pair being in a fixed position. The setup is then tuned in the same manner as the previous with initial coupling done with VLL and fine-tuned with 1550 nm tunable laser.

This results in a similar, result of 3.5 – 4 dB coupling loss. If I use this setup for coupling out of PCF into SMF the results are again similar as before with 17 dB coupling loss. Again, it is caused by the use of 3-axis stage and inability to correct the angular difference of SMF and PCF, as can be seen in Fig. 6.2.2.

6.3 Measurement of stimulated Brillouin scattering

Since I work with high input optical power there is a possibility of crossing the threshold of stimulated Brillouin scattering (SBS) as described in chapter 2.8. To experimentally determine the threshold of SBS and to test the limit of optical power which can be launched into the studied PCF I used setup that is depicted in Fig. 6.3.1.

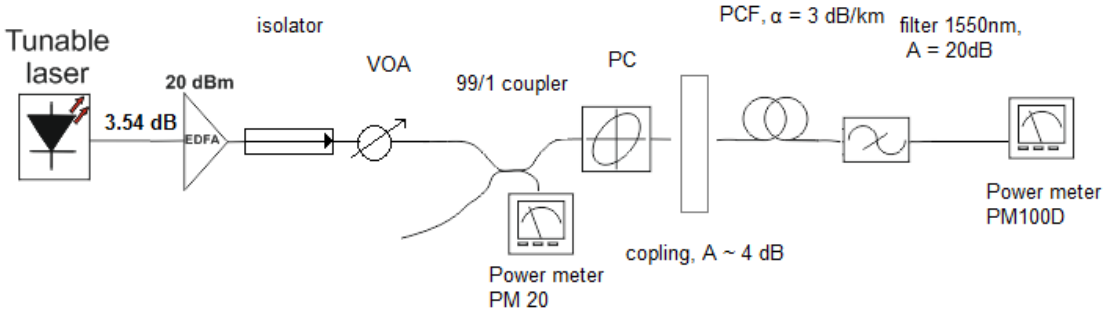

Fig. 5.3.1: Setup used to measure SBS and maximum input power

This setup uses a tunable laser with output set at 1550 nm, 6 dBm and the optical power entering EDFA at 3.54 dBm. EDFA is then used to amplify the input to 20 - 30 dBm. To measure lower power than 20 dBm I use VOA to tune power entering fiber under test.

I then use 99:1 coupler to measure precise power entering PCF under test. The power meter (PM20) connected to 1% output is used to measure the power entering PCF. As an output power meter I use Thorlabs PM100D that has large and easily positioned photodetector however, it has a damage threshold of 16 dBm. To overcome this limitation, I used filter with attenuation of 20 dB at 1550 nm.

To determine the SBS threshold I compare the values of input from power meter PM20 and output from power meter PM100D. I then change the input power linearly by 1 dBm increments, the output changes linearly as well. The results can be seen in Fig. 6.3.2.

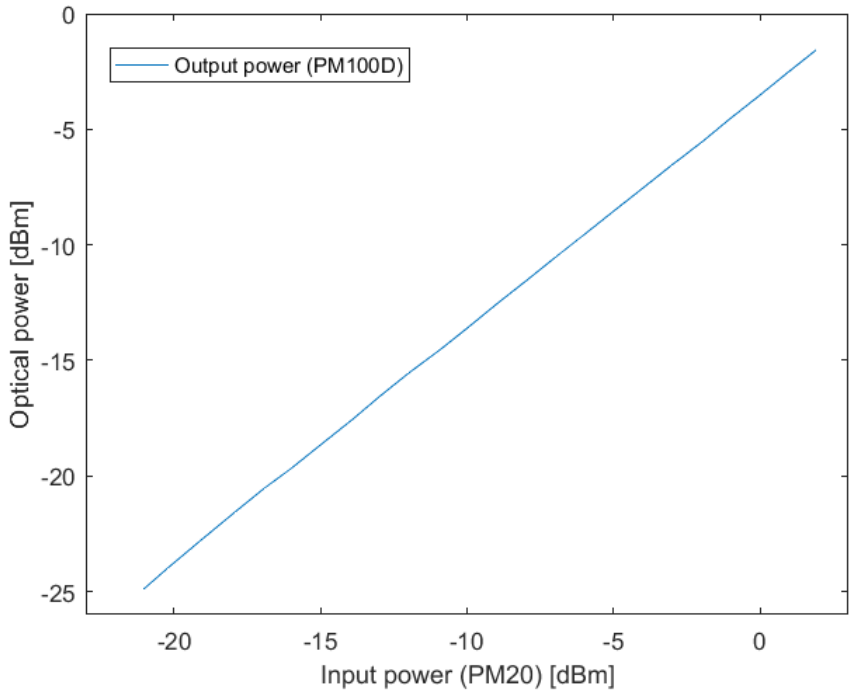

Fig. 5.3.2: Results of SBS threshold measurements.

As can be seen in Fig 5.3.2. output power has linear progression in regard to input power, and therefore no SBS was observed.

6.4 Supercontinuum generation setup and results

As described in chapter 4.3 the SC generation requires high nonlinearity and thus high input power. Therefore, before I start, it is important to thoroughly clean all connectors or these connectors or even some other equipment can be damaged as a result.

For this measurement I used PCF fiber PBG – 08 NL24-C4 made out of lead-bismuth-galate oxide glass with 1.89 refractive index, as was simulated in chapter 5. The length of the fiber is 50 cm and the picture of the fiber cross section can be seen in Fig. 6.4.1. Fiber NL29C6 was not experimentally measured due to insufficient supply of this particular fiber.

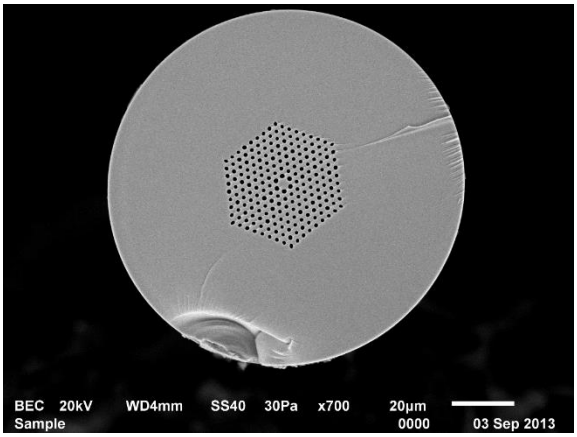

Fig. 6.4.1: Photo of the fiber used to generate SC (PBG – 08 NL24-C4) at 60x magnitude.

The entire setup will be placed on an optical table for higher stability and efficiency of coupling and can be seen in Fig. 3.4.1.

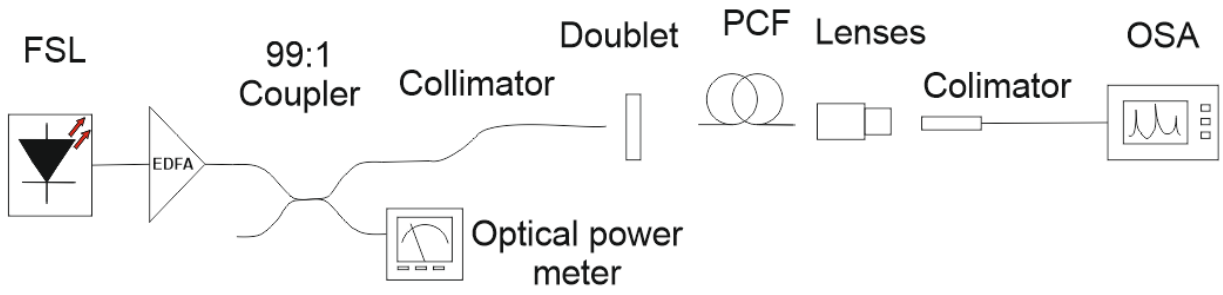

Fig. 6.4.1: Setup for SC generation.

In this setup I use FSL as described in chapter 6.1. This allows for pulse generation of 1.5 ps with 167 W peak power output and 40 MHz at 1560 nm. Since the power output of FSL is insufficient to generate SC I use EDFA (Keyopsys CEFA-C) which is able to amplify signal to 20 – 30 dBm. However, this amplifier is not designed to amplify such short pulses and as a result the spectrum of the FSL is severely distorted.

For this measurement I used OSA Yokogawa AQ6370C with 73 dB dynamic range at -10 dBm reference. The OSA is connected to 99:1 coupler is used to view the distorted spectrum of FSL after EDFA. Alternatively, OSA can be substituted by power meter to verify the power entering PCF.

To couple signal into the PCF I used coupling with a doublet and to couple the signal out of PCF I used GRIN collimator with setups described in chapter 6.2. This resulted in ~4 dB attenuation when coupling into the PCF and 23 dB attenuation when coupling out of PCF. To measure the value of PCF attenuation, I measured the PCF at two different lengths and the resulted attenuation is then calculated from the difference. For NL24C4 I measured attenuation as $\alpha = 3$ dB/m.

To generate SC, I then tuned EDFA output from 20 dBm up to 26 dBm with 1 dB increments. The results can be seen in Fig. 6.4.4 and 6.4.5.

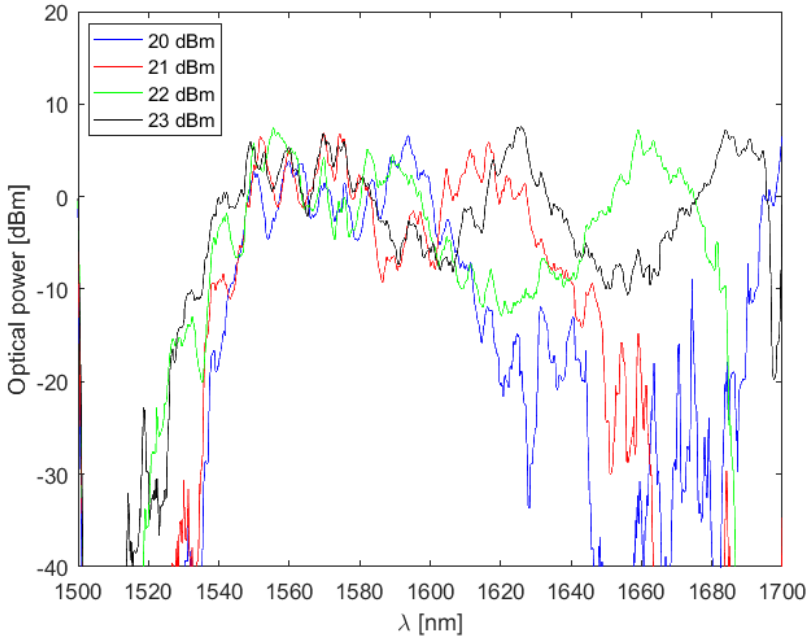

Fig. 6.4.4: The resulted generated SC with 20, 21, 22 and 23 dBm EDFA output.

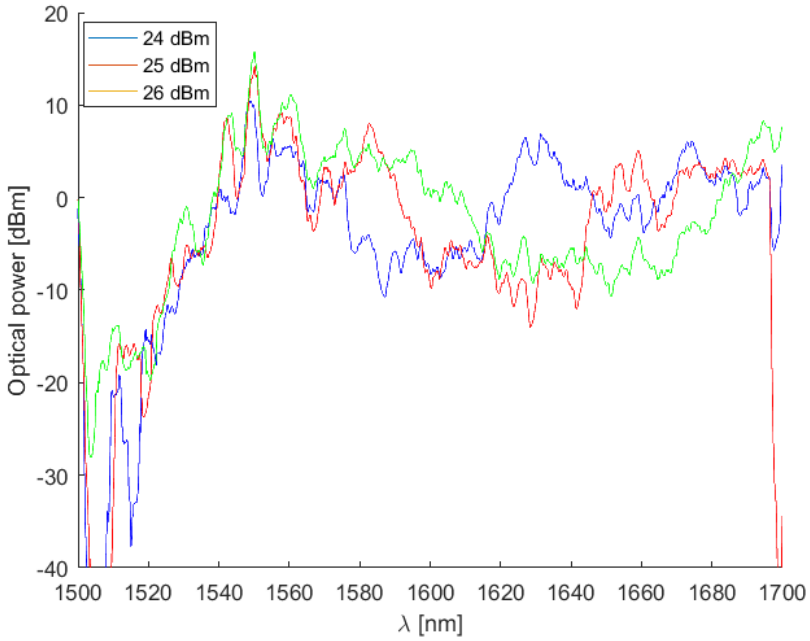

Fig. 6.4.5: The resulted generated SC with 24, 25 and 26 dBm EDFA output.

As can be seen in Fig. 6.4.4 and 6.4.5. there is apparent development of new wavelengths in the longer wavelength region. The OSA used offers maximum wavelength of 1700 nm. From the Fig. above it is apparent that the longer wavelength limit of the OSA was reached at 23 dBm. Further increase of EDFA output did not generate new wavelength components at the shorter wavelengths.

The ripple of the SC is ~20 dB across spectrum. The SC spectral span is from 1510 – 1700 nm for EDFA output of 23 dBm and more. For 20, 21 and 22 dBm EDFA output, the spectral span is 1530 – 1630, 1530 – 1665 and 1520 – 1690 respectively.

In comparison to simulation these results proved inferior in SCG, especially for shorter wavelengths. This can be contributed to the ZDW of the PCF, which is at 1982 nm and therefore is not optimal for generation of SC when 1560 nm pump is used. This conclusion was also shown during simulations which match the measured results.

Another factor is pump pulse distortion caused by EDFA. To overcome this challenge I would require either different FSL with shorter pulse duration and higher peak power or a specifically designed short pulse amplifier.

7. Conclusion

In theoretical part of this thesis I studied separately linear and nonlinear phenomena that contribute to the generation of the supercontinuum. However, the discrete description of each effect cannot fully describe the process of spectral broadening. While the initial broadening can be described by SPM and dispersion the edges of SC require different approach.

Therefore, it is important to understand the dynamics in which each of these effects interact in order to generate additional spectral components on the short and long end wavelengths.

SC generation is highly dependent on the nonlinearity and the dispersion curve of a particular optical fiber. For that reason it is useful to use PCFs as they provide possibility to tailor both these parameters, while modifying the design of the air-hole structure.

In Chapter 5 I modelled two lead-silicate fibers available, NL24C4 and NL29A6, to estimate the possibility of SCG. The result of simulations showed that it is theoretically possible to generate SCG, however it would require high-intensity peak powers.

In the experimental campaign I then proceeded with SCG. This resulted in new components being generated. However, there is significant limitation imposed by the power output of FSL, limited at 13 dBm of average output power.

While amplification of the input pulse significantly improves the SCG, as is proved by simulations, in the measurement campaign, the EDFA that I used was not designed for ultrashort pulse amplification, thus severely distorted the pulse shape. A modified amplification scheme would be required or a higher peak-power FSL source, i.e. with shorter pulses in order of hundreds of femtoseconds.

Another limitation was given by the employed OSA. Although it provided a dynamic range of 73 dB at -10 dBm reference level, it is limited by the 1700 nm at maximum wavelength. With the tuning of the EDFA this upper wavelength limit was reached at 23 dBm EDFA output and there was no reason to continue increasing EDFA power output, as there would be no possibility of displaying the results.

The measured PCF provides ZDW at 1982 nm and as result is not optimal for SCG, since I used 1560 nm pump wavelength and this conclusion was reinforced by simulations.

However even with these limitations, I generated new spectral components at the longer wavelength region up to 1700 nm and up to 1510 nm at shorter wavelength region at 23 dBm EDFA average power output. The spectral power ripple of the SC was at ~20 dB. Similar results were achieved for this fiber in simulations.

By simulating two PCFs and experimentally measuring one of them I therefore completed the thesis assignment. Future work will continue with pumping scheme over 2000 nm to fully unlock the potential of NL24C4 PCF as was observed in simulations.

8. References

[1] Dudley, J.M. and Taylor J.R. *Supercontinuum generation in optical fibers*. New York: Cambridge University Press, 2010. ISBN 0-521-514800-4.

[2] Agrawal G. P. *Fiber-optic communication systems*. 3rd ed. New York: Wiley-Interscience, 2002. ISBN 04-712-2114-7.

[3] Toroundis, T. *Fiber Optic Parametric Amplifiers in Single and Multi Wavelength Applications*. Göteborg, Sweden, 2006. Thesis for the degree of Doctor of Philosophy. CHALMERS UNIVERSITY OF TECHNOLOGY.

[4] Poli, F., Cucinotta A. and Selleri, S. *Photonic crystal fibers: properties and applications*. Dordrecht: Springer, 2007. Springer series in materials science, v. 102. ISBN 1402063253.

[5] Bananej, A. *Photonic Crystals.* InTech, 2015. ISBN 978-953-51-2121-3

[6] Paschotta, R. *Supercontinuum Generation*. In: RP Photonics Consulting GmbH [online]. [cit. 2016-05-10]. Available: https://www.rp-photonics.com/supercontinuum_generation.html

[7] Kaminski, C.F., R.S. Watt, A.D. Elder, J.H. Frank, J. Hult. *Supercontinuum radiation for applications in chemical sensing and microscopy*. Applied Physics B. 2008, 92(3), 367-378 ISSN 0946-2171.

[8] Kumar, V.V., Ravi, A., George, W., Reeves, J., Knight, P., Russel, F., Omenetto, A. T., *Extruded soft glass photonic crystal fiber for ultrabroad supercontinuum generation*. Optics Express. 2002, 10(25), ISSN 1094-4087.

[9] Hilligsøe, K. M., Andersen, T.V., Paulsen, H.N., et al. *Supercontinuum generation in a photonic crystal fiber with two zero dispersion wavelengths*. Optics Express [online]. 2004, 12(6), ISSN 1094-4087.

[10] Paschotta, R., Group Velocity Dispersion. In: RP Photonics Consulting GmbH [online]. [cit. 2016-04-10]. Available: https://www.rp-photonics.com/group_velocity_dispersion.html

[11] *Fiber Characterization and Testing Long Haul, High Speed Fiber Optic Networks* [online]. The Fiber Optic Association, Inc., 2012 [cit. 2016-05-10]. Available: http://www.thefoa.org/tech/ref/testing/test/CD_PMD.html

[12] Paschotta, R., *Chromatic Dispersion*. In: RP Photonics Consulting GmbH [online]. [cit. 2016-04-10]. Available: https://www.rp-photonics.com/chromatic_dispersion.html

[13] Paschotta, R., *Effective Mode Area*. In: RP Photonics Consulting GmbH [online]. [cit. 2016-04-10]. Available: https://www.rp-photonics.com/effective_mode_area.html

[14] Billington, R., *Effective Area of Optical Fibres - Definition and Measurement Techniques*, National Physics Laboratory [online]. [cit. 2016-05-10]. Available: http://www.npl.co.uk/upload/pdf/aeff_ver3.pdf

[15] *Nonlinear optical effects in glass-air PCF*. Max Planck Institute for science in light: Photonic Crystal Fibre science [online]. [cit. 2016-05-10]. Available: http://www.mpl.mpg.de/en/russell/research/topics/nonlinear-optics.html

[16] *Nonlinear Photonic Crystal Fibers*. Thorlabs [online]. 2016 [cit. 2016-05-10]. Available: https://www.thorlabs.com/newgrouppage9.cfm?objectgroup_id=2044

[17] Paschotta, R., *Self-phase Modulation*. In: RP Photonics Consulting GmbH [online]. [cit. 2016-04-10]. Available: https://www.rp-photonics.com/self_phase_modulation.html

[18] Marciu, D., *Optical Limiting and Degenerate Four-Wave Mixing in Novel Fullerenes*. Blacksburg, Virginia, 1999. Dissertation. Virginia Polytechnic Institute and State University. Available: http://scholar.lib.vt.edu/theses/available/etd-022299-083514/unrestricted/CHAPTER3.PDF

[19] Aso, O., Masateru T., Shu N., *Four-Wave Mixing in Optical Fibers and Its Applications*. Furukawa Review, No. 19. 2000 [online]. [cit. 2013-12-26]. Available: http://furukawa.jp/review/fr019/fr19_12.pdf

[20] Sobon, G., Klimczak, M., Sotor, J., Krzempek, K., Pysz, D., Stepien, R., Martynkien, T., Abramski, K.M. and Buczynski, R. (2014) '*Infrared supercontinuum generation in soft-glass photonic crystal fibers pumped at 1560 nm*', Optical Materials Express, 4(1), pp. 7–15. doi: 10.1364/OME.4.000007.

[21] Paschotta, R., *Raman Gain*. In: RP Photonics Consulting GmbH [online]. [cit. 2016-04-10]. Available: https://www.rp-photonics.com/raman_gain.html

[22] Sibilia, C. *Photonic crystals: physics and technology*. Milano: Springer, 2008. ISBN 8847008433.

[23] Buczynski. R., *Photonic Crystal Fibers* [online]. Warsaw University, Information Optics Group, Faculty of Physics, Poland, 2004 [cit. 2016-05-10]. Available: http://przyrbwn.icm.edu.pl/APP/PDF/106/a106z216.pdf.

[24] Mortensen, N.A., *Effective area of photonic crystal fibers*. Optics Express. 2002, 10(7), 341-348.

[25] Paschotta, R., *Photonic Bandgap Fibers*. In: RP Photonics Consulting GmbH [online]. [cit. 2016-04-10]. Available: https://www.rp-photonics.com/photonic_bandgap_fibers.html

[26] Chen, Y.-S., Yan, P.-G., Chen, H., Liu, A.-J. and Ruan, S.-C. (2015) '*Harmonic mode-locked fiber laser based on Photonic crystal fiber filled with Topological insulator solution*', Photonics, 2(2), pp. 342–354.

[27] Ramsay, R. (2007) *Sensing & measurement* [online]. [cit. 2016-04-10]. Available: http://spie.org/newsroom/1371-photonic-crystal-fiber-characteristics-benefit-numerous-applications.

[28] Ruffin, B., *Stimulated Brillouin Scattering: An Overview of Measurements*, System Impairments, and Applications. [online] 2004 [cit. 2014-05-12]. Available at: http://www.corning.com/docs/corporate/discovery_center/innovation_library/2004/NTRNTR100886_NIST_SOFM_Ruffin.pdf

[29] Singh, S.P., Gangwar, R., Singh., N., "*Nonlinear scattering effects in optical fibers*", Progress In Electromagnetics Research, Vol. 74, 379-405, 2007

[30] Gladyshev, A.V., Kolyadin, A.N., Kosolapov, A.F., Yatsenko, Y.P., Pryamikov, A.D., Biryukov, A.S., Bufetov, I.A. and Dianov, E.M. (2015) '*Efficient 1.9-μm Raman generation in a hydrogen-filled hollow-core fibre*', Quantum Electronics, 45(9). doi: 10.1070/qe2015v045n09abeh015881.

[31] Roberts, P., Couny, F., Sabert, H., Mangan, B., Williams, D., Farr, L., Mason, M., Tomlinson, A., Birks, T. Knight, J., Russell, P. St. J., "*Ultimate low loss of hollow-core photonic crystal fibres,*" Opt. Express 13, 236-244 (2005) http://www.opticsinfobase.org/oe/abstract.cfm?URI=oe-13-1-236

[32] Choi, J.H., Shi, F.G., Margaryan, A., Margaryan, A. and Nieh, T.G., "*Dopant and concentration dependence of linear and nonlinear refractive index and dispersion for new (Mg, Ba)F2 based fluorophosphates glass*" T.G. AFO Research Inc. [online]. [cit. 2016-05-10] Available: http://www.aforesearch.com/info/11-final.pdf

[33] Klimczak, M., B. Siwicki, P. Skibinski, et al., *Mid-infrared supercontinuum generation in soft-glass suspended core photonic crystal fiber*. Optical and Quantum Electronics ,2014, 46(4), p.p. 563-571.

[34] Kyunghwan. O., Paek, U., *Silica optical fiber technology for devices and components: design, fabrication, and international standards*. Hoboken, N.J.: Wiley, c2012. ISBN 9780471455585.

[35] Liu, S., Liu, W., Niu, H. (2015) '*Supercontinuum generation with Photonic crystal fibers and its application in Nano-imaging*', in Photonic Crystals. InTech,

[36] Zhao-lun, L., Lan-tian, H., Wei, W. (2009) '*Tailoring nonlinearity and dispersion of photonic crystal fibers using hybrid cladding*', Brazilian Journal of Physics, 39(1).

[37] Tombelaine, V., Labruyère, A., Kobelke, J., Schuster, K., Reichel, V., Leproux, P., Couderc, V., Jamier, R. and Bartelt, H. (2009) '*Nonlinear photonic crystal fiber with a structured multi-component glass core for four-wave mixing and supercontinuum generation*', Optics Express, 17(18), p. 15392.

[38] Liu, S. and Li, S.-G. (2013) '*Numerical analysis of photonic crystal fiber with chalcogenide core tellurite cladding composite microstructure*', Chinese Physics B, 22(7), p. 074206.

[39] Miret, J. J., Silvestre, E., Andrés. P., "*Octave-Spanning Ultraflat Supercontinuum With Soft-Glass Photonic Crystal Fibers*". Opt. Express 17.11 (2009): 9197.

[40] Sysoliatin, A.A., Senatorov, A.K., Konyukhov, A.I., Melnikov, L.A. and Stasyuk, V.A. (2007) '*Soliton fission management by dispersion oscillating fiber*', Optics Express, 15(25), p. 16302.

[41] *Evolutional Properties of Localized Excitations for Generalized Broer–Kaup System in (2+1) Dimensions*, Scientific Figure on ResearchGate. Available from: https://www.researchgate.net/231147536_fig1_Fig-1-The-evolutional-profile-of-one-soliton-fission-into-two-solitons-for-the-field-g

[42] Paschotta, R., *Nonlinear Polarization Rotation*. In: RP Photonics Consulting GmbH [online]. [cit. 2016-04-10]. Available: https://www.rp-photonics.com/nonlinear_polarization_rotation.html

[43] Lei, T. et al., "*Numerical Study On Self-Similar Pulses In Mode-Locking Fiber Laser By Coupled Ginzburg-Landau Equation Model*". Opt. Express 17.2 (2009)

[44] Xu, H., *Nonlinear Polarization Rotation for Fiber Lasers with Ultra High Pulse Energy*. [cit. 2016-04-10]. Available at: http://www.optics.unm.edu/sbahae/physics568/studentpapers2011/Xu.pdf

[45] Broeng, J., Bjarklev, A., Libori, S.E.B., Folkenberg, J.R., Vienne, G. and A, C.F. *(2002) Patent US7590323 - optical fibre with high numerical aperture, method of its production, and use thereof*. Available at: http://www.google.com/patents/US7590323 (Accessed: 20 May 2016).